© 2022. Published by The Company of Biologists Ltd | Development (2022) 149, dev200026. doi:10.1242/dev.200026

RESEARCH ARTICLE

The topography of corticopontine projections is controlled by postmitotic expression of the area-mapping gene *Nr2f1*

Chiara Tocco[1,*], Martin Øvsthus[2,*], Jan G. Bjaalie[2], Trygve B. Leergaard[2,‡] and Michèle Studer[1,‡]

ABSTRACT

Axonal projections from layer V neurons of distinct neocortical areas are topographically organized into discrete clusters within the pontine nuclei during the establishment of voluntary movements. However, the molecular determinants controlling corticopontine connectivity are insufficiently understood. Here, we show that an intrinsic cortical genetic program driven by *Nr2f1* graded expression is directly implicated in the organization of corticopontine topographic mapping. Transgenic mice lacking cortical expression of *Nr2f1* and exhibiting areal organization defects were used as model systems to investigate the arrangement of corticopontine projections. By combining three-dimensional digital brain atlas tools, *Cre*-dependent mouse lines and axonal tracing, we show that *Nr2f1* expression in postmitotic neurons spatially and temporally controls somatosensory topographic projections, whereas expression in progenitor cells influences the ratio between corticopontine and corticospinal fibres passing the pontine nuclei. We conclude that cortical gradients of area-patterning genes are directly implicated in the establishment of a topographic somatotopic mapping from the cortex onto pontine nuclei.

KEY WORDS: Corticopontine topography, Layer V pyramidal neurons, Gradients of area mapping genes, Nr2f1, Conditional knockout mouse models, *Thy1*-e*YFP-H* reporter line, Pontine nuclei, 3D data analysis, 3D digital brain atlas, Anterograde fluorescent tracing

INTRODUCTION

Neuronal populations responsible for fine motor coordination are arranged in topographically organized maps in the neocortex and cerebellum, with different body parts being represented in largely continuous maps in the somatosensory cortex (Chapin and Lin, 1984; Fabri and Burton, 1991; Welker, 1971; Woolsey and Van der Loos, 1970), but in discontinuous fractured maps in the cerebellum (Bower, 2011; Bower et al., 1981; Bower and Kassel, 1990; Leergaard et al., 2006; Nitschke et al., 1996; Shambes et al., 1978). The intercalated regions of this network, the pontine nuclei, deep cerebellar nuclei and thalamus, receive and integrate signals, ultimately resulting in coordinated and seamlessly executed behaviours (Buckner, 2013; Peterburs and Desmond, 2016; Stoodley and Schmahmann, 2010), including fine voluntary movements (Badura et al., 2013; Mottolese et al., 2013).

The pontine nuclei constitute the major synaptic relay for cerebro-cerebellar signals (Brodal and Bjaalie, 1992; Lemon, 2008; Mihailoff et al., 1985). Axonal projections originating from layer V pyramidal neurons across the neocortex are distributed in topographically organized clusters within the pontine nuclei, as shown in monkey (Brodal, 1978; Schmahmann and Pandya, 1997), cat (Bjaalie and Brodal, 1997), rat (Leergaard et al., 2000a,b) and, to some extent, mouse (Henschke and Pakan, 2020; Inoue et al., 1991; Proville et al., 2014). Within the pontine nuclei, the three-dimensional (3D) arrangement of clustered terminal fields, well described in rats, both preserves the overall topographical relationships of the cortical maps, and partially overlaps and introduces new spatial proximities among projections from different cortical areas (Bjaalie and Brodal, 1989; Leergaard, 2003; Leergaard and Bjaalie, 2007).

To date, the mechanisms responsible for establishing the topographic map between the neocortex and pontine nuclei are poorly understood. The leading proposition, referred to as chrono-architectonic hypothesis, postulates that the complex 3D topography is a product of straightforward spatio-temporal gradients, possibly combined with non-specific chemo-attractive mechanisms (Leergaard, 2003; Leergaard and Bjaalie, 2007; Leergaard et al., 1995). Recent new discoveries raise the possibility that other mechanisms are also in action during the establishment of the corticopontine maps. Several lines of evidence suggest a functional role of graded gene expression during topography of sensory maps in several systems (D'Elia and Dasen, 2018; Erzurumlu et al., 2010; Fritzsch et al., 2019; McLaughlin and O'Leary, 2005), but whether this process is also operative during establishment of corticopontine topography is not understood. A recent study has shown that postmitotic graded expression of the HOX gene *Hoxa5* is directly involved in imparting an anterior-to-posterior identity to pontine neurons and in attracting corticopontine axons (Maheshwari et al., 2020). Whether gradient expression of molecular factors along the antero-posterior or medio-lateral axes of the cerebral cortex also intrinsically determines the topography of corticopontine projections is still not known.

Layer V neurons from the anterolateral cerebral cortex project to the central regions of the pontine nuclei, while more medially located cortical regions project to more external parts; motor area projections are distributed more medially and rostrally, while somatosensory projections reach the middle and caudal parts of the pontine nuclei. Finally, auditory and visual cortical projections innervate the dorsolateral regions of the pontine nuclei (Leergaard et al., 2004; Leergaard and Bjaalie, 2007). The fine-tuned and precise corticopontine topography raises the possibility that cortical neurons

[1]University Côte d'Azur, CNRS, Inserm, iBV, Nice 06108, France. [2]Institute of Basic Medical Sciences, University of Oslo, Oslo N-0317, Norway.
*These authors contributed equally to this work

‡Authors for correspondence (michele.studer@unice.fr; t.b.leergaard@medisin.uio.no)

C.T., 0000-0002-2616-0198; M.Ø., 0000-0002-6175-1647; J.G.B., 0000-0001-7899-906X; T.B.L., 0000-0001-5965-8470; M.S., 0000-0001-7105-2957

Handling Editor: James Briscoe
Received 16 July 2021; Accepted 20 December 2021

Development (2022) 149, dev200026. doi:10.1242/dev.200026

are intrinsically programmed to target specific groups of pontine neurons, possibly coupling both intrinsic and extrinsic mechanisms to direct proper topographical innervation to the pontine nuclei.

A new theme of cortical patterning has emerged, in which genetic factors direct the spatial and temporal establishment of topographically organized axonal connections between the cortex and subcortical brain regions (Cadwell et al., 2019). Area-mapping genes are expressed in gradients along the different axes of the cortical primordium, and are known to modulate the size and position of future cortical areas (Alfano and Studer, 2012; Cadwell et al., 2019; O'Leary and Sahara, 2008). They also determine areal fate and regulate expression of downstream molecules that, in turn, control the topographic organization of synaptic inputs and outputs of related structures (Assimacopoulos et al., 2012; Greig et al., 2013). These genes represent good candidates for modulating topographic mapping. In mice, the *Nr2f1* gradient expression appears to be a particularly strong candidate for having a formative role during the establishment of topographic maps (Armentano et al., 2007; Liu et al., 2000; Zhou et al., 2001). For example, *Nr2f1* is expressed in cortical progenitor cells from embryonic day E9.0 in a high caudo-lateral (future sensory) to low rostro-medial (future motor) gradient fashion, which is maintained in postmitotic descendants and postnatally, when the cortical area map is completed (Bertacchi et al., 2019; Flore et al., 2017; Tomassy et al., 2010). Previous studies show that *Nr2f1* promotes somatosensory (S1) cortex identity by repressing motor identity in postmitotic neurons; in its absence, area size and thalamocortical topography are both affected (Alfano et al., 2014; Armentano et al., 2007; Bertacchi et al., 2019). We thus hypothesized that *Nr2f1* could control topographic corticopontine mapping during corticogenesis.

To this purpose, we made use of cortico-specific *Nr2f1* conditional knockout mice as an *in vivo* model system and a paradigm to investigate the contribution of cortical genetic programs in the establishment of topographic corticopontine projections. Two distinct conditional mouse lines were crossed to the *Thy1*-e*YFP-H* reporter line (Feng et al., 2000), in which YFP is highly expressed in cortical layer V pyramidal neurons and their axonal projections (Porrero et al., 2010). The distribution of fluorescent YFP signals as well as anterogradely labelled corticopontine projections were evaluated by comparison of spatially corresponding microscopic images and 3D visualization of extracted point-coordinate data representing labelling. Our results indicate that cortical *Nr2f1* expression plays a dual role in controlling the spatio-temporal development of corticopontine projections. Although early expression in progenitor cells influences the ratio between corticofugal fibres passing the pontine nuclei, loss of postmitotic late expression specifically affects topographic pontine mapping. Overall, our data demonstrate that intrinsic genetic programs and postmitotic graded expression of cortical area-mapping genes are implicated in the establishment of area-specific targeting of corticopontine neurons.

RESULTS

Benchmark 3D topographic organization of corticopontine projections in wild-type mice

To first establish a 3D reference of the topographical organization of corticopontine projections in wild-type adult mice, we used tract tracing data from the Allen Institute Mouse Brain Connectivity Atlas (Wang et al., 2020), see flowchart in Fig. 1A. These data allowed us to visualize the spatial distribution of the pontine projections of motor and somatosensory neocortical areas. Corticopontine projections digitized from sagittally oriented

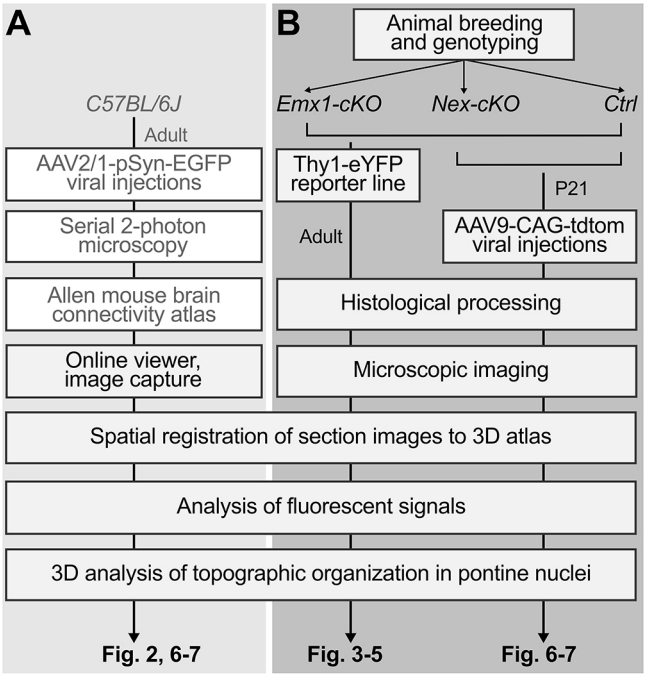

Fig. 1. Experimental and analytic workflow. (A) Workflow for generating a 3D topographic map of corticopontine projections in wild-type mice using tract tracing data from the Allen Mouse Brain Connectivity Atlas, mapped and compared in a 3D reference atlas space. Steps performed by the Allen Institute are indicated with grey text in white boxes. (B) The two paradigms investigated in cKO models, with the analytic steps performed in adult control, *Emx1-cKO* and *Nex-cKO* mutant animals, and the tract tracing of the 3D topography of motor and somatosensory corticopontine projections in young control and *Nex-cKO* mutants. All images were spatially registered to the Allen Mouse Brain Atlas (CCFv3; Wang et al., 2020) prior to analyses, to facilitate comparison of images and spatial distribution patterns. Results are shown in Figs 2-7.

microscopic images (matching the orientation used for our experimental data, see below) were co-visualized as 3D data points in a 3D viewer tool (see, for example, Fig. 2A-D). Experimental data were selected and coloured according to tracer injection localizations in the cerebral cortex: first, to visualize and compare the pontine distribution of corticopontine projections from motor and somatosensory areas; and, second, to determine the organization of projections arising from progressively more medial and caudal locations in the cerebral cortex, following the cortical neurogenetic gradient that ripples out from the anterolateral cortex (Leergaard and Bjaalie, 2007; Smart, 1984). Our findings confirm that the somatosensory and motor neurons of the mouse cortex project to largely separate parts of the pontine nuclei (Henschke and Pakan, 2020; Inoue et al., 1991; Proville et al., 2014), with clustered terminal fields topographically distributed in the same concentric fashion (Fig. 2L-P) as previously reported in rats (Leergaard et al., 2000a; Leergaard and Bjaalie, 2007). These 3D point data were also used below as additional control data, and as benchmarks for interpreting YFP expression and tract-tracing results in *Nr2f1* mutant mice.

Area-specific layer V neuron distribution in cortices lacking Nr2f1

To assess the influence of cortical area mapping on the establishment of topographical organization in mouse corticopontine projections, we used *Nr2f1* conditional knockout mice as an experimental model

Development (2022) 149, dev200026. doi:10.1242/dev.200026

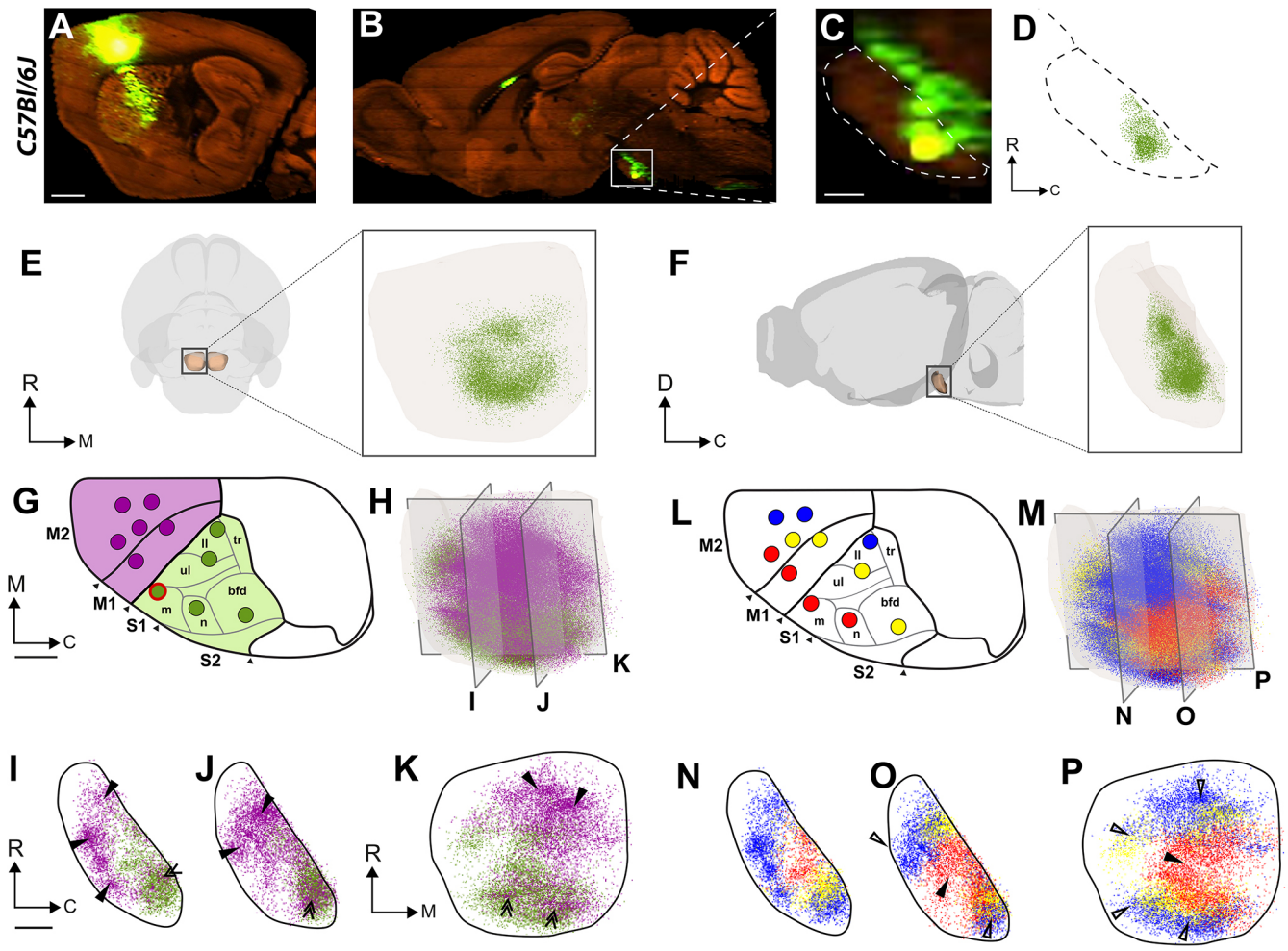

Fig. 2. Topographical organization of corticopontine projections in wild-type mice. (A-D) Representative example illustrating the data acquisition of corticopontine projections labelled by viral tracer injection in the S1 face representation of a wild-type mouse from the Allen Mouse Brain Connectivity Atlas. The tracer injection site centre (A) and anterogradely labelled axons in the pontine nuclei (B,C) are shown in sagittal microscopic images. (D) Dot map representation showing semi-quantitatively recorded points corresponding to the density of labelling observed in the section shown in C. (E,F) The 3D point populations recorded from the example case, together with a transparent surface rendering of the right pontine nuclei, seen from ventral (E) and medial (F) views. The S1 corticopontine projections are distributed in dense clusters located centrally in the pontine nuclei. (G-P) Differently coloured 3D visualizations of point clouds representing spatial distribution of anterogradely labelled corticopontine axons derived from 11 experiments available in the Allen Mouse Brain Connectivity Atlas, injected with the anterograde tracer EGFP in the primary (M1)/secondary (M2) motor cortex (purple dots) or primary somatosensory (S1) cortex (green dots), at locations indicated with colour coded circles in G and L. (H,M) 3D visualizations of all points in the right pontine nuclei, colour coded as indicated in G and L. A grid of transparent grey planes indicates the position and orientation of ~100 µm digital slices cut with sagittal and frontal orientations through the point clouds, shown in I-K,N-P. The red circle in G indicates the tracer injection site shown in A. (G-K) Point clouds showing that motor and somatosensory areas largely target different parts of the pontine nuclei, with projections from M1 and M2 (purple dots) located more peripherally towards rostral, ventral and medial than projections from S1 (green dots), as indicated by arrowheads in I-K, but also that motor and sensory projections overlap caudally in the pontine nuclei (double arrowheads in I-K). (L-P) 3D co-visualization of all data points colour-coded in red, yellow or blue according to the location of the cortical injection sites from anterolateral (red) progressively towards medial or posterior (yellow, blue). The slices through the point clouds reveal a concentric arrangement in the pontine nuclei, with projections from the anterolateral parts of the M1/M2 and S1 located centrally and medially (filled arrowheads in O,P), and projections from more medial and posterior cortical locations progressively shifted towards rostral, caudal and lateral (unfilled arrowheads in O,P). bfd, barrel field; C, caudal; D, dorsal; ll, lower limb; m, mouth; M1, primary motor cortex; M2, secondary motor cortex; n, nose; R, rostral; S1, primary somatosensory cortex; S2, secondary somatosensory cortex, tr, trunk; ul, upper limb; V, ventral. Scale bars: in A, 1 mm for A,B; in C, 200 µm for C; in G and I, 200 µm for G,L and I-K,N-P, respectively.

system and their littermates as controls (Alfano et al., 2014; Armentano et al., 2007). Two well-established conditional *Nr2f1* mouse mutants were used: the *Nr2f1*$^{fl/fl}$*::Emx1-Cre* mouse, in which *Nr2f1* expression is abolished from early cortical progenitor cells at mouse embryonic stage (E) 9.5 (Armentano et al., 2007); and the *Nr2f1*$^{fl/fl}$*::Nex-Cre* mouse, in which *Nr2f1* expression is inactivated at later stages (E11.5-E12), solely in cortical postmitotic neurons (Alfano et al., 2014; Goebbels et al., 2006). Both mouse lines were crossed to the *Thy1-eYFP-H* reporter line to specifically restrict signal expression to layer V pyramidal neurons (Harb et al., 2016; Porrero et al., 2010). In these mice, YFP expression follows the physiological distribution of subcortical layer V projections, including corticospinal and corticopontine fibres, with a high density in motor cortex and a gradually decreased distribution in S1 and more caudal areas. For simplicity, *Nr2f1*$^{fl/fl}$*::Emx1-Cre* and *Nr2f1*$^{fl/fl}$*::Nex-Cre* are referred to as *Emx1-cKO* and *Nex-cKO*, respectively.

In agreement with a previous study (Porrero et al., 2010), we observed substantial YFP signal expression in the hippocampus, tectum and pontine nuclei, as well as in the globus pallidus, claustrum, endopiriform nucleus, nucleus of the lateral olfactory tract,

Development (2022) 149, dev200026. doi:10.1242/dev.200026

mammillary nuclei, piriform area and the substantia innominata in adult mice (Fig. 3A). Signal expression was also seen in the vestibular nuclei, deep cerebellar nuclei and cerebellum. Although YFP expression was present in almost the same cortical regions in 2-month-old mutant mice as in controls, detailed analysis of layer V expression revealed some distinct differences in the spatial distribution of *Emx1-cKO* and *Nex-cKO* brains relative to their respective controls, and between the two conditional lines. We used an ImageJ macro to automatically count YFP$^+$ nuclei by area of interest in the brain using a threshold based on intensity and shape of the elements. This allowed us to estimate the number of YFP$^+$ neurons in seven cortical areas (corresponding to prefrontal, motor, somatosensory, auditory, visual and retrosplenial cortices in control mice) defined by delineations from spatially registered overlay images from the Allen Mouse Brain Atlas (Wang et al., 2020) (Fig. 1; Fig. 3B-D′). In control animals, the number of YFP$^+$ neurons follows the physiological distribution of subcortical layer V projections (Fig. 3B,B′), as previously reported (Polleux et al., 1997; Porrero et al., 2010; Shepherd, 2009). Strong staining in motor and somatosensory cortices resulted in bright signal expression in the cerebral peduncle (CP) and corticospinal tract (CST) (Fig. 3A).

To understand whether the spatial organization of YFP$^+$ layer V cortical neurons was affected upon loss of cortical *Nr2f1* gradient expression, we quantified and compared the number of YFP$^+$ cells across mutant and control brains (Fig. 3E,F). As previous reports showed that the distribution of layer V neurons changes in the absence of Nr2f1 (Alfano et al., 2014; Armentano et al., 2007; Tomassy et al., 2010), we expected that the Thy1-YFP signal would also be altered, as a read-out of layer V changes. Indeed, the layer V gradient was disrupted in both mutant strains, and YFP$^+$ cells were more homogenously distributed along the antero-posterior cortical axis (Fig. 3B-F). Although *Emx1-cKO* brains showed a significant increase in YFP$^+$ cells in parietal and occipital regions, compared with controls, this was not the case for *Nex-cKO* brains, which instead revealed a decrease in only frontal areas (Fig. 3F). To better quantify the differences between corticopontine projections from frontal and parietal areas, where normally the motor and somatosensory areas develop (Leergaard et al., 2000a,b), we compared the ratio of YFP$^+$ cells over the total cell populations counted in the frontal (motor) and parietal (somatosensory) areas (Fig. 3G). We found that the percentage of YFP$^+$ cells was significantly decreased in frontal (motor) cortex and concomitantly increased in parietal (somatosensory) cortex in both *Emx1-cKO* and *Nex-cKO* compared with controls, but no differences were found between the two lines (Fig. 3E,G). This lack of a difference in the distribution of YFP$^+$ layer V neurons between cortical regions normally containing the motor and somatosensory areas is in line with the acquisition of a motor-like identity in the somatosensory cortex of Nr2f1-deficient brains, as previously reported (Alfano et al., 2014). We next asked whether and how alterations in layer V organization observed in the two mutant lines would be translated into layer V corticospinal projections and/or corticopontine topographic mapping.

Abnormal corticospinal projections and fasciculation in *Nr2f1* mutant brains

We hypothesized that the disordered cortical distribution of YFP-expressing layer V neurons in mutant mice might influence the integrity of subcortical axonal projections. In all cases, strong YFP signal expression was seen bilaterally in the main corticofugal pathways (Fig. 3A), visible as longitudinally oriented fibre bundles coursing towards the CP (Fig. 4A-D), passing dorsal to the pontine nuclei as the longitudinal fasciculus (Fig. 4B′-D′), and continuing through the brain stem towards the spinal cord as the CST. Because a large fraction of the corticobulbar fibres terminate in the pontine nuclei (Tomasch, 1968, 1969), we reasoned that abnormal distribution of YFP$^+$ layer V neurons observed in mutant mice (Fig. 3) might affect corticopontine innervation, and could be reflected by an abnormal size of the pontine longitudinal fascicle as it enters the CP and exits the pons in rostral and caudal positions to the pontine nuclei, respectively. To evaluate this, we measured the dorso-ventral width of the longitudinal fascicle of the pons in sequential sections along the medio-lateral axis. The measurements were taken at rostral and caudal levels to the pontine nuclei (Fig. 4A′). Surprisingly, we found the lateral part of the fascicle to be wider at both rostral and caudal levels in *Nex-cKO* mice compared with *Emx1-cKO* and controls, while being narrower medially (see red area chart in Fig. 4E,F), suggesting that the longitudinal fascicle of the pons is flattened and expanded laterally upon Nr2f1 inactivation in postmitotic neurons. Only minor differences were observed in the *Emx1-cKO* fascicles (blue area chart in Fig. 4E,F). This is also supported by quantification of the total surface of the longitudinal fascicle of the pons at rostral and caudal levels, which shows a significant surface area reduction at caudal levels, but only a tendency towards a reduced surface area at rostral levels, in *Emx1-cKO* mice (Fig. 4G,H). These data indicate that genetic inactivation of *Nr2f1* in cortical progenitors, but not in neurons, results in fewer YFP$^+$ fibres passing the pontine nuclei towards the brain stem to form the CST.

Moreover, we observed, caudal to the pontine nuclei, abnormally widespread fibre fascicles in the CST of mutant animals (arrowheads in Fig. 4C′,D′). To determine whether there was a significant difference between animal groups, we estimated the degree of fibre bundle fasciculation in the CST of *Emx1-cKO* and *Nex-cKO* mice. At locations of 250 µm and 500 µm caudal to the pontine nuclei (Fig. 4A′), we measured the total dorso-ventral width of the CST at several medio-lateral levels and subtracted the gaps between the YFP-expressing fibre bundles at the same levels. The ratio of the total width of the CST and fibres was used as a measure of the fasciculation index (Fig. 4I). Notably, in both groups of mutant mice, we found a lower degree of fasciculation in the CST that was more pronounced at the most caudal level (Fig. 4I). Together, these data show that loss of *Nr2f1* expression affects the diameter, shape and degree of fasciculation of the CST originating from layer V neurons.

Dual role of Nr2f1 in targeting corticopontine projections

Next, we evaluated whether topographical organization of corticopontine projections depended on proper cortical area mapping and layer V distribution (Fig. 5). To achieve this, we assessed the spatial distribution of YFP signal expression within the pontine nuclei by comparing intensity-normalized microscopic images of spatially corresponding sagittal sections from the brains of *Emx1-cKO*, *Nex-cKO* and control littermate animals (Fig. 1B; Fig. 5A). A complete documentation of spatially comparable and reproducible images is provided in Figs S1 and S2. In control brains, we observed a strong YFP signal in central parts of the pontine nuclei, with the densest expression surrounding a centrally located zone exhibiting less-dense signals (Fig. 5B-E). This region of the pontine nuclei typically receives strong projections from somatosensory areas (green dots in Fig. 2G-K). Some signal expression was also visible in medial parts of the pontine nuclei (Fig. 5D,E), which receive projections primarily from cortical motor areas (purple dots in Fig. 2G-K). By contrast, signal expression was lower in rostral and lateral parts of the pontine nuclei (Fig. 5B,C,E),

Development (2022) 149, dev200026. doi:10.1242/dev.200026

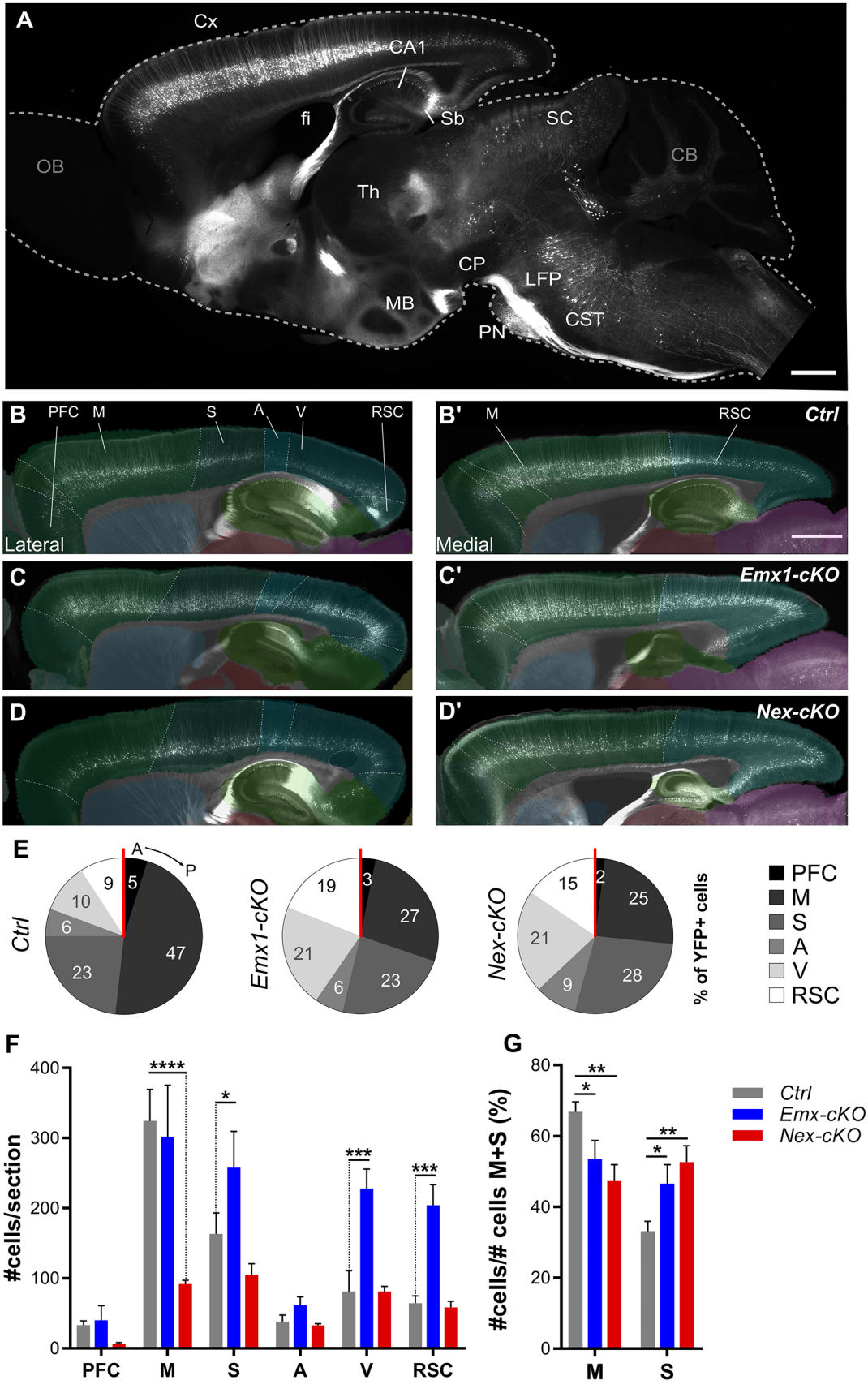

Fig. 3. See next page for legend.

Development (2022) 149, dev200026. doi:10.1242/dev.200026

Fig. 3. Distribution of YFP-positive layer V pyramidal neurons in cerebral cortex of control, *Emx1-cKO* and *Nex-cKO* adult brains. (A) Fluorescence microscopy image of a representative sagittal section from control brain, showing widespread YFP expression. (B-D′) Fluorescence microscopy images of lateral (B-D) and medial (B′-D′) sagittal sections of *Ctrl* (B,B′), *Emx1-cKO* (C,C′), and *Nex-cKO* (D,D′) brains, with spatially corresponding *CCFv3* atlas diagrams superimposed to indicate the location of cortical areas. (E) Pie charts illustrating the distribution of YFP$^+$ layer V neurons in different cortical areas along the antero-posterior axis of controls and mutant brains. (F) Graph showing the number of YFP$^+$ neurons across cortical areas in adult *Ctrl* (grey), *Emx1-cKO* (blue) and *Nex-cKO* (red) mice normalized for the total sections analysed. (G) Graph showing a subsampling of the analysis in E. Here, the number of YFP$^+$ layer V neurons in frontal (motor; M) and parietal (somatosensory; S) areas are normalized for the sum of YFP$^+$ cells of M and S regions only, and the values are presented as percentages. Data were analysed with two-way-ANOVA test (see also Tables S4, S6), and are illustrated as mean±s.e.m. (*Ctrl*, *n*=6; *Emx1-cKO*, *n*=4, *Nex-cKO*, *n*=4). A, auditory cortex; CA1, cornu ammonis area 1; CB, cerebellum; CP, cerebral peduncle; CST, corticospinal tract; Cx, cortex; fi, fimbria; GC, gustatory cortex; LFP, longitudinal fascicle of the pons; M, motor areas (includes primary and secondary motor cortices); MB, mammillary body; OB, olfactory bulb; PFC, prefrontal cortex; PN, pontine nuclei; RSC, retrosplenial cortex; S somatosensory areas; SC, superior colliculus; Sb, subiculum; Th, thalamus; V, visual cortex. Scale bars: 1 mm in A; 500 µm in B-D′.

known to receive projections from visual and auditory areas of the cerebral cortex (Inoue et al., 1991; Leergaard and Bjaalie, 2007).

Interestingly, *Emx1-cKO* mice showed a relatively homogeneous signal distribution across all parts of the pontine nuclei, and displayed more expression in the dorso-lateral regions (Fig. 5F-I). Signal expression was also present in the medial part of the nuclei (Fig. 5G-I). This observation fits well with the finding of a higher number of YFP$^+$ neurons in the occipital cortex (Fig. 3C,C′,F), which projects to the dorso-lateral pontine nuclei. By comparison, *Nex-cKO* animals showed more-constrained signal expression that predominated in rostrally and caudally located clusters extending from the cerebral peduncle towards the ventral surface of the pons, and medially surrounding a central core with low expression (Fig. 5J-M). These clusters were more peripherally located than those observed in control animals (Fig. 5J-M). Notably, little signal expression was seen in the central region of the pontine nuclei of all *Nex-cKO* cases (unfilled arrowheads in Fig. 5J-L), despite the presence of YFP$^+$ layer V neurons in somatosensory cortex (Fig. 3D,D′,F,G). This central region is normally innervated by projections from the face representations located in S1 (Fig. 2A-F).

Taken together, these findings show that corticopontine projections are abnormally distributed in Nr2f1-deficient mice, with more homogenously (non-specific) distributed expression in *Emx1-cKO* mice (schematically summarized in Fig. 5N,O), and more peripherally distributed signal expression in *Nex-cKO* mice, which display reduced expression in the central region of the pontine nuclei that normally receives somatosensory projections (schematically summarized in Fig. 5N,P; Figs S1 and S2). In both mutant groups, the signal expression was expanded to dorso-lateral regions of the pontine nuclei that normally are innervated by projections from occipital cortical areas. This suggests that cortical *Nr2f1* graded expression in postmitotic neurons might be directly involved in the establishment of topographically organized corticopontine projections.

Altered somatosensory topographic projections in *Nex-cKO* adult mutant mice

To further support that *Nr2f1* gradient cortical expression might be directly involved in topographical pontine mapping, we focused on the *Nex-cKO* genetic model to unveil the cortical origin of the innervation defect. Compared with the *Emx1-cKO* mice, in which projections are more disorganized and abundant, the *Nex-cKO* mouse model exhibits externally shifted projections, more suitable for investigating changes in topographical mapping using experimental tract tracing techniques. Therefore, we injected the AAV9-CAGtdTomato anterograde viral tracer (Pourchet et al., 2021) in the cortex of 5-day-old (*P5*) *Nex-cKO* mice and littermate controls, in frontal and parietal locations corresponding to the motor or S1 areas in control mice, respectively (Figs 6 and 7). The mice were then sacrificed at P21 and brain sections analysed microscopically (Fig. 1B). All histological sections were spatially registered to the Allen Mouse Brain Atlas (common coordinate framework, CCF3; Wang et al., 2020), and the location of tracer injections sites were mapped in the same atlas space (Figs 6A and 7A). For each injection site location in a *Nex-cKO* brain, we selected the most corresponding control experiment or wild-type tract-tracing data from the Allen Mouse Brain Connectivity Atlas as additional controls. Representative examples of injections and comparisons between controls and littermate *Nex-cKO* brains are shown in Figs 6B-C′ and 7B-C′. Complete documentation of all tracing experiments cases is provided in Figs S3-S5.

In controls, the spatial distributions of corticopontine projections (dark grey point clouds in Figs 6 and 7) were highly comparable with the labelling patterns seen in corresponding wild-type tracing data from the Allen Mouse Brain Connectivity Atlas (Wang et al., 2020). As expected, tracer injections into areas corresponding to the motor cortex in control mice gave rise to labelled axonal clusters located rostrally, caudally and medially in the pontine nuclei (purple dots in Figs 2G-K and 6D-F; Figs S3 and S4). In all *Nex-cKO* mice receiving tracer injections into areas normally corresponding to the motor cortex, the overall distribution of corticopontine labelling was found to be essentially similar to that observed in control cases (compare grey point with red point clouds in Fig. 6D-F; Figs S3-S5).

Tracer injections into S1 areas of control animals gave rise to labelled axonal clusters located centrally or caudally in the pontine nuclei (grey point clouds in Fig. 7D-I). The spatial distribution of labelling varied systematically as a function of the location of the cortical injection sites, such that (1) the face representation in the lateral part of S1 projects centrally in the pontine nuclei (Fig. 7G,H; Fig. S3I,J), (2) the whisker representations lateral and more posterior in S1 project to regions surrounding the central core (Fig. 7F; Fig. S3K), while (3) the more medially located forelimb and hindlimb representations of S1 projected to medio-laterally oriented regions in the caudal part of the pontine nuclei (Fig. 7D,E; Fig. S3G,H). By contrast, tracer injections in *Nex-cKO* brains, at locations corresponding to control S1 representations of the whiskers or upper limb, or into the S1/M1 (sensorimotor) lower limb representation, gave rise to abnormal distribution of corticopontine fibres (Fig. 7D-G). Specifically, corticopontine projections from medial parts of parietal cortex (corresponding to the S1 forelimb and hindlimb representations in control mice) were shifted towards more rostral locations in *Nex-cKO* experiments (Fig. 7D-F, red points), resembling the distributions observed after tracer injections into motor areas in the control experiments (Fig. 6D-F).

Notably, tracer injections placed in the antero-lateral parietal cortex in *Nex-cKO* mice, in regions normally representing sensory surfaces of the head, gave rise to labelled axons distributed in the central part of the pontine nuclei, with more subtle difference to the matching control experiments (Fig. 7G). In two *Nex-cKO* cases,

Development (2022) 149, dev200026. doi:10.1242/dev.200026

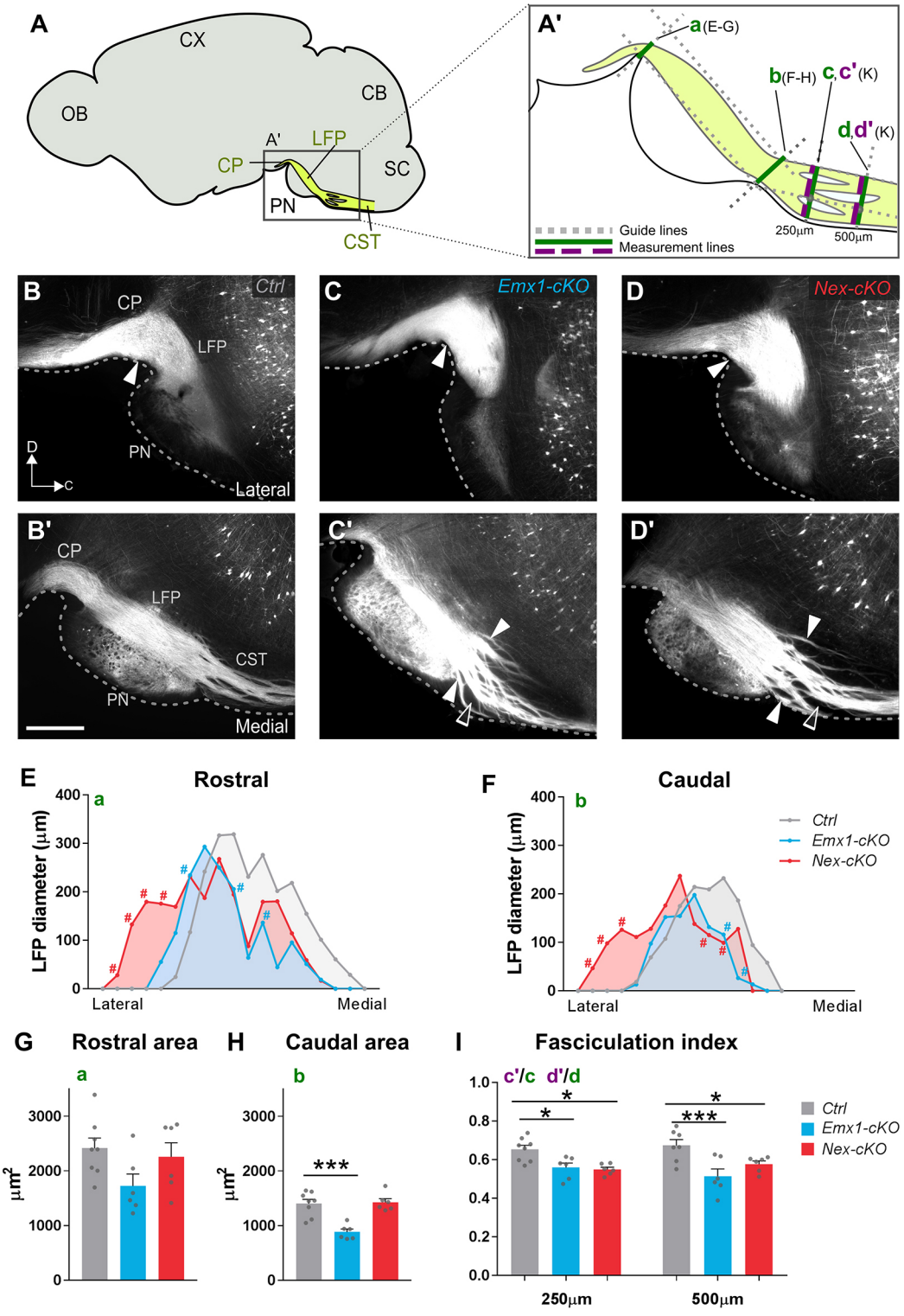

Fig. 4. See next page for legend.

projections from regions corresponding to the S1 head representation were distinctly medially shifted, relative to control experiments (red dots in Fig. 7G,I), attaining a distribution resembling corticopontine projections from head representations in M1 cortex, located significantly more anteriorly in the cortex (grey dots in Fig. 7I). Interestingly, two tracer injections in similar locations, corresponding to the border between nose and whisker representations, gave rise to labelling located in central and rostral parts of the pontine nuclei (Fig. 7F,G, red dots, see also Fig. 7C′) with predominantly rostrally shifted fibres in one case (Fig. 7F,C′; Fig. S5J), and centrally located and medially shifted fibres in the other case (Fig. 7G; Fig. S5K). Despite the differences in density distributions, both cases represent a distinct shift of fibre distributions towards regions normally receiving motor

Development (2022) 149, dev200026. doi:10.1242/dev.200026

Fig. 4. Loss of Nr2f1 function leads to abnormal corticospinal projections and fasciculation. (A) Schematic diagram of a sagittal mouse brain section showing the location of the pontine nuclei (PN) and descending fibre tracts (yellow) in the cerebral peduncle (CP), longitudinal fascicle of the pons (LFP) and corticospinal tract (CST). (A′) Diagram illustrating the different measurements shown in E-I. (B-D′) Fluorescence microscopy images of sagittal sections showing the corticospinal tract entering the LFP (B-D) and continuing caudal to the pons as the CST (B′-D′). White arrowheads indicate the sites of measurement plotted in E and F, respectively. Rostrally, the labelled LFP has similar thickness in the three genotypes. Caudally, the CST features defasciculation of fibre bundles (white arrowheads in C′,D′ indicate thinner and more dispersed bundles in *Emx1-cKO* and *Nex-cKO* mutants); empty arrowheads indicate empty spaces between bundles. (E,F) Plots showing LFP diameter measurements obtained from lateral to medial before and after innervating the PN (rostral and caudal, respectively). Each measurement represents the average value of corresponding sections among distinct animals and each position on the *x*-axis represents a specific section of the series. (G,H) Graphs showing average values of the area under the curves in E,F. A comparable number of fibres reach the CP in the three genotypes (G). In *Emx1-cKO* brains, fewer fibres are seen to exit at the level of the pons compared with control and *Nex-cKO* brains (H). (I) Graph showing CST fasciculation index, based on measurements of total thickness and fibre thickness (green and purple line respectively in A′) performed at 250 and 500 µm from the terminal edge of the PN. A ratio between the two measurements was calculated for each position. Data are mean±s.e.m. Data were analysed with a two-way ANOVA (E,F) or a one-way ANOVA (G-I) and corrected for multiple comparison with the Bonferroni test (see also Tables S4, S6). *Ctrl*, *n*=8; *Emx1-cKO*, *n*=6; *Nex-cKO*, *n*=6. #P<0.05 in E,F. *P<0.05 and ***P<0.005 in G-I. CB, cerebellum; CX, cortex; OB, olfactory bulb; SC, spinal cord. Scale bar: 500 µm.

projections. Taken together, our observations indicate that corticopontine projections from antero-lateral cortex in *Nex-cKO* mice display abnormal topographical distributions resembling the normal mice projections from homologous representations in the more anterior and medially located primary motor cortex of control mice. Finally, one tracer injection placed in the most antero-lateral part of S1 in a *Nex-cKO* mouse, at a location corresponding to the perioral surface representation in controls, yielded corticopontine labelling highly similar to that of a control experiment (Fig. 7H).

Our findings show that corticopontine projections from frontal (motor) areas and the most antero-laterally located parts of the parietal (S1) cortex are topographically similar in *Nex-cKO* and control brains, whereas corticopontine projections from most parts of the parietal cortex, where head, whisker, upper limb and lower limb representations of S1 are located in control mice, are abnormally shifted towards rostral and medial regions of the pontine nuclei, normally receiving projections from cortical motor areas (schematically summarized in Fig. 7J,K). This is in overall agreement with the spatial and temporal control of *Nr2f1* in area mapping. Indeed, the absence of changes in corticopontine projections from the frontal (motor) cortex might be due to low *Nr2f1* expression in this area (spatial control), whereas lack of changes in the projections originating from the most antero-lateral part of the parietal (S1) cortex, from which the earliest cortical projections to innervate the forming pontine nuclei originate, might be explained by the late *Nr2f1* genetic inactivation occurring after the earliest layer V neurons have been produced (temporal control).

DISCUSSION

Our present study questions whether and how spatio-temporal cortical expression gradients are involved in the establishment of normal topographical organization of corticopontine projections. By combining genetically modified mice and public mouse brain connectivity data with tract-tracing techniques and digital brain atlas tools, we have provided novel evidence of an intrinsic molecular control of layer V cortical neurons during the establishment of topographical organization of corticopontine projections. Abnormal areal organization in the neocortex induced by *Nr2f1* inactivation is reflected in altered corticopontine projections, as well as impaired structural integrity of the CST. Although loss of *Nr2f1* from the early progenitor cell pool leads to increased and abnormal corticopontine innervation at the expense of corticospinal projections, only late postmitotic *Nr2f1* inactivation reveals altered topographic pontine mapping from medially located parts of somatosensory cortex controlling whisker and limb representations. No shifts in projections from the earliest generated antero-lateral cortical areas were observed in these mice, in line with a spatial and temporal control of *Nr2f1* expression, respectively. Overall, our data show that proper area mapping of the neocortical primordium is a pre-requisite for preserving the cortical spatial and temporal segregation within the pontine nuclei, and thus correct corticopontine topographic organization.

Spatial accuracy of topographical data compared across experiments

To ensure accurate 3D data in wild-type and genetically modified mice, we relied on spatial alignment of serial microscopic section images to a common reference atlas achieved through non-linear image registration method (Puchades et al., 2019). The use of non-linear registration compensated for minor shape differences among brains and allowed comparison of distribution patterns among spatially relevant data. The focus on the location rather than the amount of signal expression/axonal labelling also compensated for the variation in signal expression intensity and size of tracer injections among cases. By representing signal expression and axonal labelling as 3D point clouds, it became possible to directly explore and compare location and distribution patterns in 3D in different combinations of datasets. For the additional benchmark data extracted from the Allen Mouse Brain Connectivity Atlas (Wang et al., 2020), we used the same sagittal image orientation as in our microscopic data to facilitate comparison of microscopic images in addition to the 3D comparisons. The relevance and accuracy of the approach was confirmed by demonstrating that similarly located cortical tracer injections in control animals gave rise to similarly distributed labelling patterns in the pontine nuclei. Given the distinct patterns of topographical organization of corticopontine projections, the interpretation and comparison of spatial distribution patterns and variability in our tract tracing experiments critically depended on the analysis of tracer injection locations and on a 3D understanding of the topographical mapping of the cortical surface onto the pontine nuclei, which were derived from our analyses of control experiments and earlier studies of the rat corticopontine system (Leergaard and Bjaalie, 2007).

Mitotic versus postmitotic Nr2f1 functions in layer V corticofugal projections

Our previous work showed overall areal organization impairments in cortical *Nr2f1* mutant brains, whether *Nr2f1* inactivation was carried out in progenitors or postmitotic neurons. Here, we report for the first time that *Nr2f1* drives corticopontine connectivity differently in progenitors versus postmitotic neurons. While *Nr2f1* expressed by progenitor cells modulates the ratio between corticopontine and corticospinal axonal projections, similarly to what happens in *C. elegans* with the ortholog *UNC-55* (Petersen et al., 2011; Zhou and Walthall, 1998), postmitotic *Nr2f1* expression specifically acts on somatosensory topographic organization of

Development (2022) 149, dev200026. doi:10.1242/dev.200026

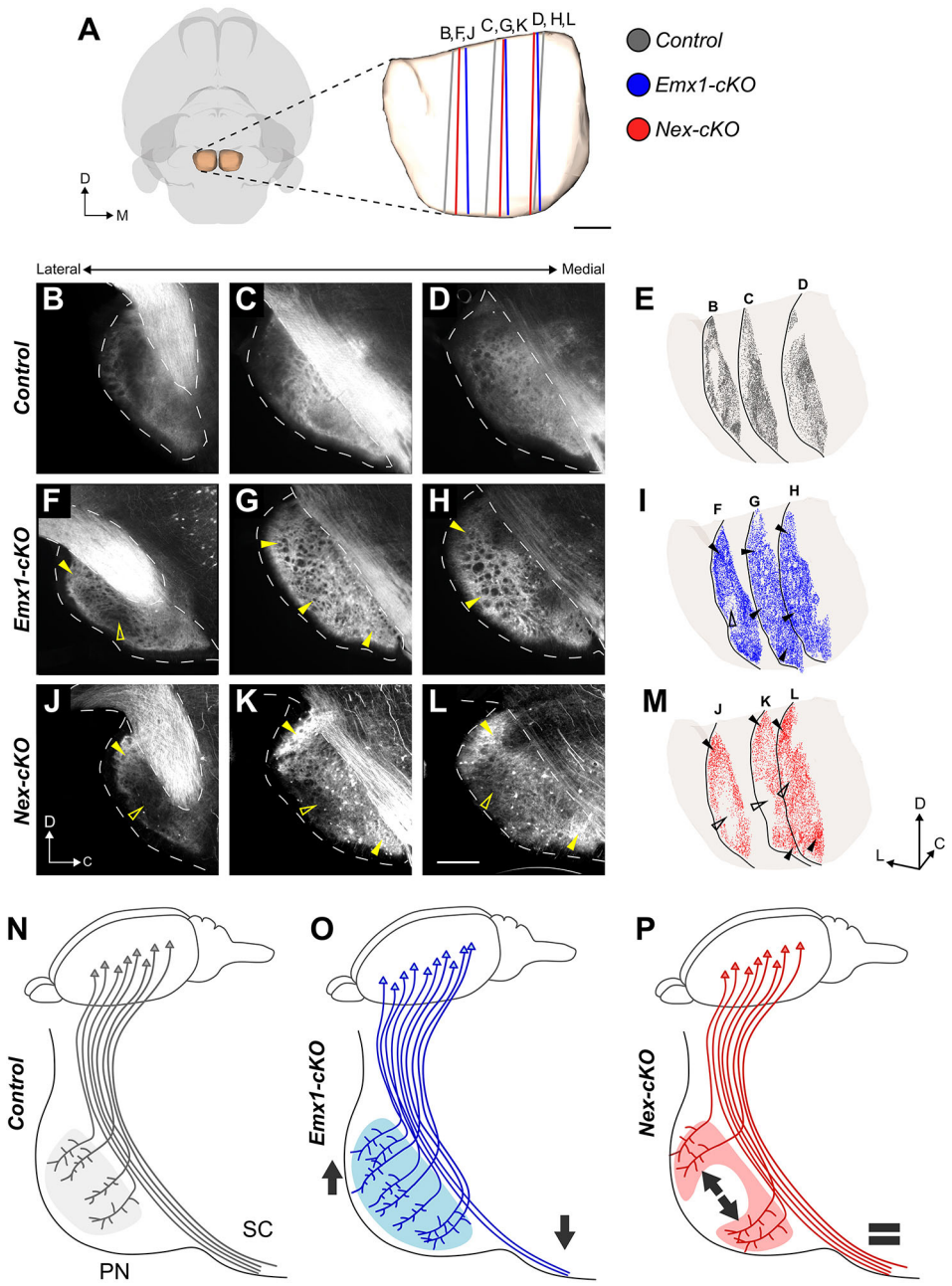

Fig. 5. Distribution of YFP signal expression in the pontine nuclei of knockout and control mice. (A) 3D representation of the outer surface of the brain (transparent grey) and pontine nuclei (PN) (transparent brown) viewed ventrally. Coloured lines indicate the location and orientation of the sagittal sections shown in B-M. (B-D,F-H,J-L) Fluorescence microscopy images of sagittal sections from corresponding medio-lateral levels of the PN, showing the spatial distribution of YFP signal expression in control, *Emx1-cKO* and *Nex-cKO* mice. (E,I,M) 3D visualization of the PN in an oblique view from ventro-medial, with point coded representations of signal expression from each of the three sagittal sections shown in B-D (E), F-H (I) and J-L (M). Filled arrowheads indicate regions with increased signal expression in mutant mice; unfilled arrowheads indicate regions with decreased signal expression. In control mice (B-E), signal expression is primarily seen in central and caudal parts of the pontine nuclei; in *Emx1-cKO* mice (F-I), signal expression is more widespread and diffuse throughout the entire PN, including more peripheral parts towards rostral, ventral and caudal positions (filled arrowheads in G-I). In *Nex-cKO* mice (J-M), signal expression is reduced in the central core region of the PN (unfilled arrowheads in K-M), while being increased in peripheral (rostral and caudal) regions. (N-P) Diagrams summarizing observed changes in corticopontine connectivity upon *Nr2f1* inactivation. In control mice (N), YFP^+ corticopontine projections primarily target the central part of the PN and a substantial number of fibres continue towards the spinal cord. In *Emx1-cKO* mutants (O), fewer fibres reach the SC and more projections target the PN (downward and upward arrows, respectively), and show a pattern of innervation more diffuse and widespread than in controls. In *Nex-cKO* animals (P), no differences between corticospinal and corticopontine projections are detected compared with controls (equal sign), but corticopontine topography appears to be affected, whereby fibres reach more-lateral, motor-receiving PN regions instead of targeting the S1-receiving core (illustrated by divergent arrows). C, caudal; D, dorsal; L, lateral; M, medial; PN, pontine nuclei; R, rostral; SC, spinal cord. Scale bar: 200 µm.

corticopontine neurons (Figs 4 and 5). This suggests that early *Nr2f1* expression in progenitor cells is mainly required in the initial axonal pathfinding of layer V subtypes, while later postmitotic expression is more implicated in the later refinement of corticopontine topographical organization. Since YFP+ cells follow the physiological distribution of subcortical layer V

Development (2022) 149, dev200026. doi:10.1242/dev.200026

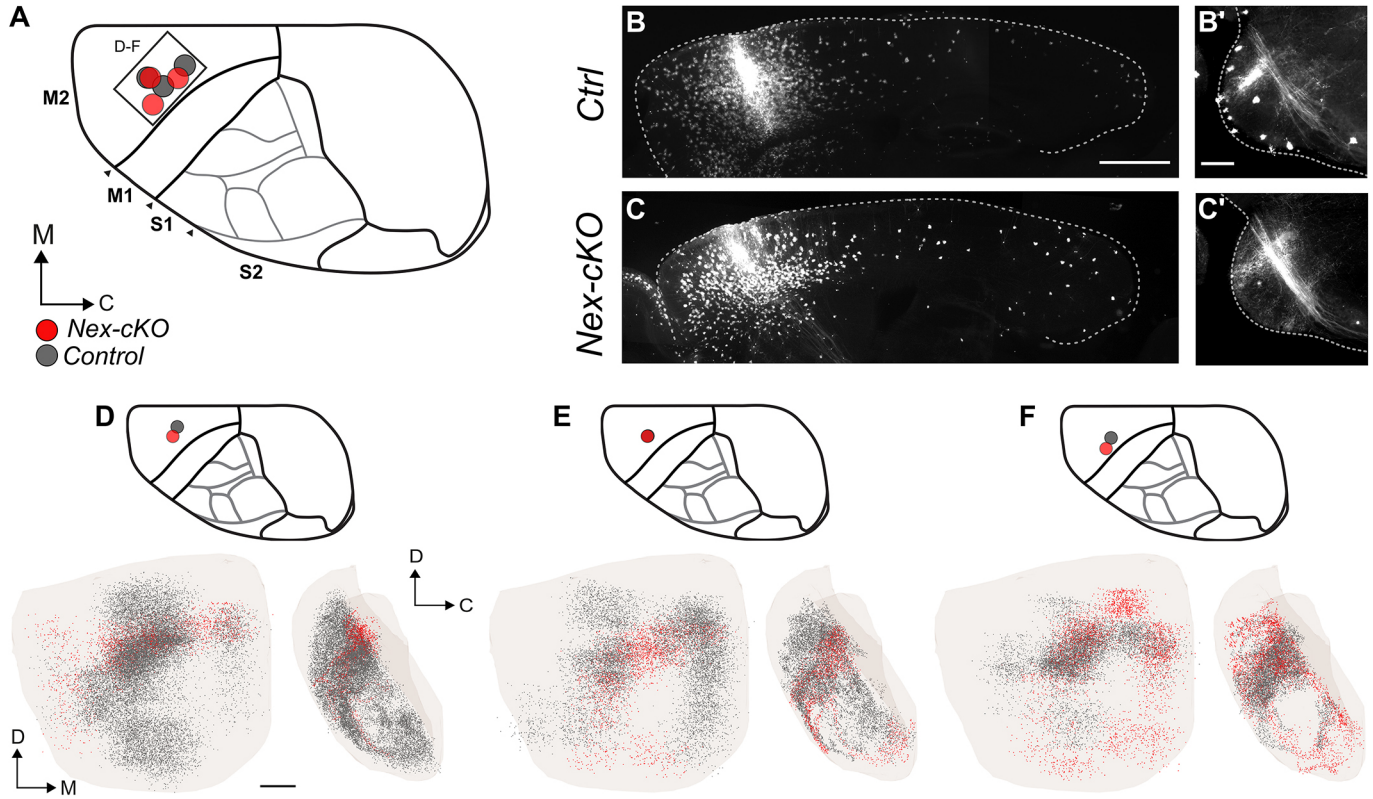

Fig. 6. Anterograde tracing of corticopontine projections from frontal (motor) areas in *Nex-cKO* mice. (A) Overview of injection sites in corresponding locations in the right frontal cortex in *Nex-cKO* (red) and control (grey) brains. The atlas diagrams shown in A, D, E and F indicate the control cortical area identities. (B-C′) Representative microscopic images of the injection site localization (B,C) and pontine nuclei innervation (B′,C′) in the control and *Nex-cKO* cases reported in F. (D-F) 3D coloured point clouds representing axonal labelling in corresponding pairs of *Nex-cKO* (red) or control/wild-type (dark grey) mice, shown within a transparent surface representation of the right pontine nuclei in ventral and medial views. Inset drawings of the brains viewed dorsally show the location of tracer injection sites for each combination of point clouds. Tracer injections in corresponding locations in frontal cortex of both *Nex-cKO* and control/wild-type mice give rise to similar corticopontine labelling in rostrally located clusters, curving towards ventral and caudal along the surface of the pontine nuclei. C, caudal; D, dorsal; M, medial; M1, primary motor cortex; M2, secondary motor cortex; S1, primary somatosensory cortex; S2, secondary somatosensory cortex. Scale bars: in B, 1 mm in B,C; in B′ and D, 200 µm in B′,C′,D.

projections (Porrero et al., 2010), Thy1-driven YFP fluorescence will be induced in cortical subpopulations related to the specificity of their axonal target region; a tight relationship which will not be altered in the conditional *KO* models. Accordingly, a higher number of layer V neurons in parietal *Emx1-cKO* cortices leads to disorganized corticopontine innervation, in accordance with increased Lmo4 expression, known to drive layer V neurons versus the pontine nuclei (Cederquist et al., 2013; Harb et al., 2016). By contrast, *Nex-cKO* parietal axonal projections reach pontine targets normally innervated by motor-derived cortical areas. Finally, increased number of YFP^+ cells in visual and auditory areas in the occipital cortex, corresponds to an augmented innervation in dorso-lateral regions of pontine nuclei known to receive projections from the occipital cortex. Together, these data indicate a dual role for Nr2f1 in layer V corticofugal connectivity: an early role in subtype specification (corticopontine versus corticospinal) and a later role in topographical mapping.

Revising the chrono-architectonic hypothesis of cortico-pontine circuit development

Previous data in developing rats have shown that pontine neurons settle in the forming pontine nuclei in a shell-like fashion according to their birthdate, with early-born neurons forming the central core of the pontine nuclei, and later-born neurons consecutively settling around and forming concentric rings (Altman and Bayer, 1987). At early postnatal stages, corticopontine axons are chemotropically attracted as collateral branches from corticospinal axons (Heffner et al., 1990; O'Leary and Terashima, 1988), innervating the pontine nuclei in a topographic inside-out pattern (Leergaard et al., 1995). Neurons in the frontal (motor) cortex project rostrally and medially in the pontine nuclei, neurons in the parietal (somatosensory) cortex project to central and caudal parts, neurons in the temporal (auditory) cortex project to central and lateral regions, and neurons in the occipital (visual) cortex to lateral and rostral parts of the pontine nuclei (Leergaard and Bjaalie, 2007). This concentric organization of corticopontine projections suggests that the birthdate of pontine neurons and their inside-out genesis is linked to the spatial organization of cortical inputs. However, intrinsic differences in pontine neurons born at different times might also have an instructive role for corticopontine innervation. A recent study in mice showed that postmitotic expression of the HOX gene *Hoxa5* guides pontine neurons to settle caudally within the pontine nuclei, where they are targeted by projections from limb representations in the somatosensory cortex (Maheshwari et al., 2020). Moreover, ectopic *Hoxa5* expression in pontine neurons is sufficient to attract cortical somatosensory inputs, regardless of their spatial position, showing that pontine neurons can play an instructive and attractive role in topographic input connectivity of corticopontine neurons (Maheshwari et al., 2020).

Development (2022) 149, dev200026. doi:10.1242/dev.200026

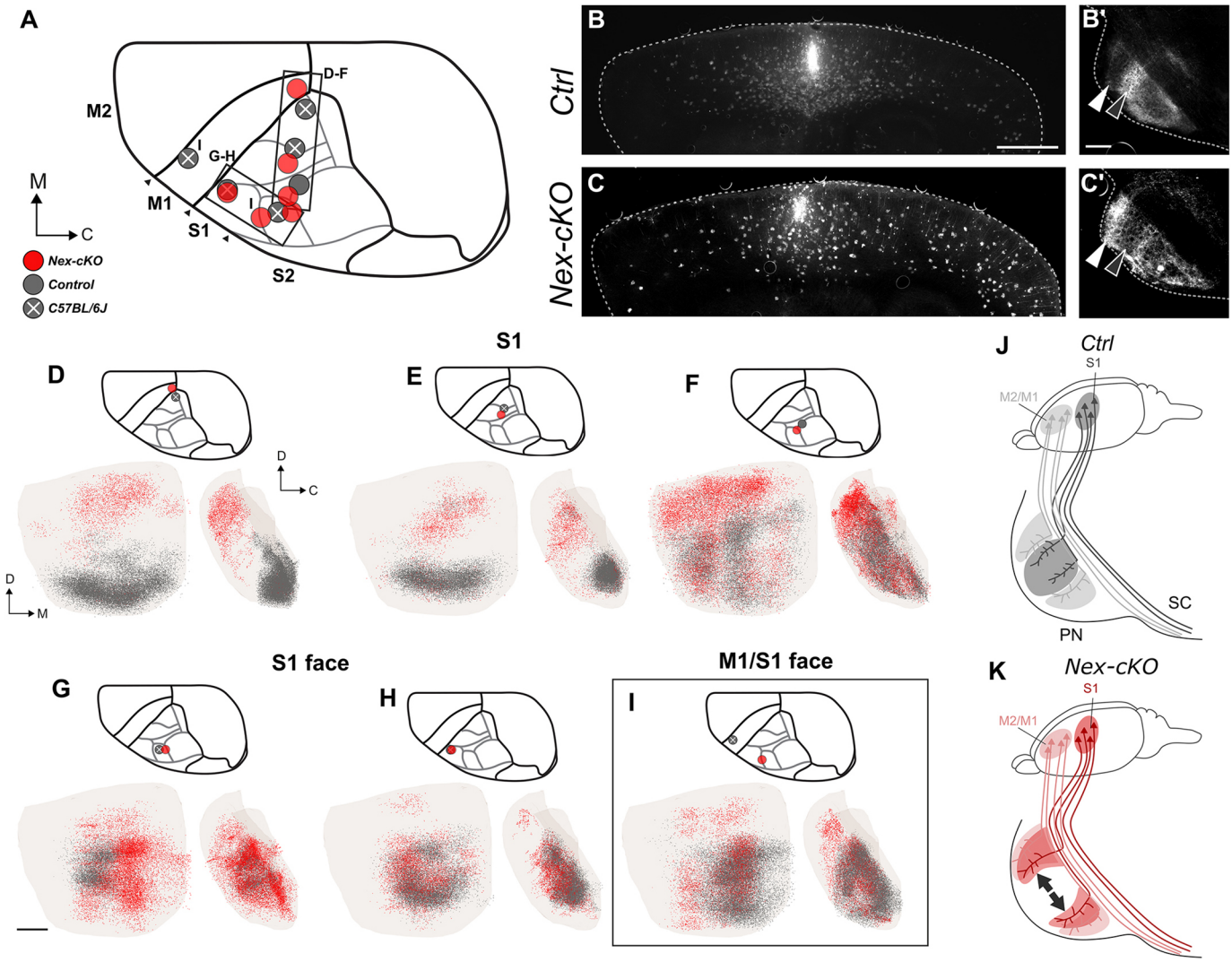

Fig. 7. Anterograde tracing of corticopontine projections from somatosensory areas in *Nex-cKO* mice. (A) Overview of injection sites in corresponding locations in the right parietal (primary somatosensory; S1) cortex in *Nex-cKO* (red), control (grey) and wild-type (grey with white cross) brains. (B-C′) Representative microscopic images of the injection site localization (B,C) and pontine nuclei innervation (B′,C′) in the control and *Nex-cKO* cases reported in F. (D-I) 3D coloured point clouds representing axonal labelling in corresponding pairs of *Nex-cKO* (red) or control/wild-type (grey) mice, shown within a transparent surface representation of the right pontine nuclei in ventral and medial views. Inset drawings of the brains viewed dorsally show the location of tracer injection sites for each combination of point clouds. Corresponding tracer injections in corresponding locations in the medial parietal cortex of *Nex-cKO* and control/wild-type mice give rise to labelling in different parts of the pontine nuclei, with corticopontine projections in control mice distributed in elongated curved clusters located caudally (grey points in D,E) or laterally in the pontine nuclei (grey points in F), while projections from the same locations in *Nex-cKO* mice are shifted to more peripheral rostral and lateral parts of the pontine nuclei (red points in D-F). All tracer injections in the anterolateral part of the parietal cortex of *Nex-cKO* and control mice, in regions corresponding to the S1 face representation in wild-type mice, gave rise to labelling in the central region of the pontine nuclei; however, there was a subtle medial shift of projections in *Nex-cKO* brains (G, see also I). Corresponding tracer injections in the most anterolateral part of S1 in a *Nex-cKO* and control gave rise to highly similar labelling, centrally in the pontine nuclei. (I) Tracer injections in widely separated locations in S1 (*Nex-cKO*) and M1 (wild-type control) gave rise to largely corresponding labelling in the medial part of the central core region of the pontine nuclei, albeit with additional rostral and medial labelling in the *Nex-cKO* experiment. (J,K) Diagrams summarizing observed changes in corticopontine connectivity upon *Nr2f1* postmitotic inactivation. In control mice (J), projections from motor areas (M2/M1, pink) and S1 (purple) target largely segregated parts of the pontine nuclei, with somatosensory projections targeting the central core region, while motor projections target more peripheral rostral, caudal and medial parts of the pontine nuclei. In *Nex-cKO* animals, corticopontine topography of S1 is affected, whereby fibres reach lateral, motor-receiving PN regions, instead of targeting the core (illustrated by grey divergent arrows). C, caudal; D, dorsal; M, medial; M1, primary motor cortex; M2, secondary motor cortex; PN, pontine nuclei; S1, primary somatosensory cortex; S2, secondary somatosensory cortex, SC, spinal cord. Scale bars: in B, 1 mm in B,D; in B′, 200 µm in B′,C′; in G, 200 µm for D-I.

Nevertheless, maturational gradients in the pontine nuclei cannot fully explain the complexity of the fine-grained somatotopic topographic connectivity pattern between cortical input and pontine neuron targets. As the establishment of topographic maps requires multiple processes and structures, it is conceivable that the position and specific intrinsic molecular programs of both presynaptic afferents and postsynaptic target neurons contribute to this complex corticopontine connectivity map. Indeed, our data show that, without affecting the development and maturation of pontine neurons, corticopontine Nr2f1-deficient layer V axons originating from the parietal S1 cortex will abnormally target the pontine region, a function normally assigned to corticopontine motor axons. By contrast, Nr2f1-deficient axons originating from the frontal and medial cortex will innervate the expected pontine

Development (2022) 149, dev200026. doi:10.1242/dev.200026

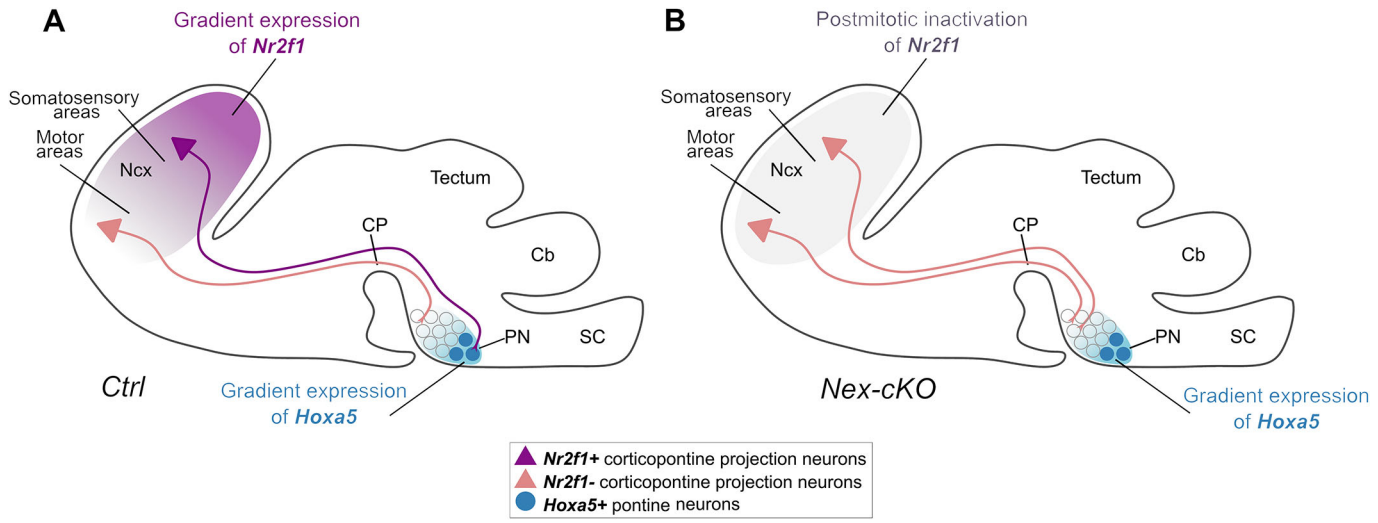

Fig. 8. Model of corticopontine topography establishment and changes upon *Nr2f1* cortical inactivation. (A) Proposed schematic model of how the neocortex (Ncx) and the pontine nuclei (PN) might interact during development in driving corticopontine topography. Both structures need to be pre-patterned by gradient expression of transcription factors. Although postmitotic pontine graded expression of *Hoxa5* will impart an anterior to posterior identity to pontine neurons (graded blue circles) (Maheshwari et al., 2020), postmitotic cortical gradient expression of *Nr2f1* (purple gradient in the Ncx) will intrinsically instruct corticopontine neurons to innervate their topographically proper targets (this study). (B) In the absence of postmitotic *Nr2f1* gradient expression in the neocortex, but maintenance of *Hoxa5* expression in the PN, axons from motor and somatosensory cortex will both innervate rostrally located clusters within the PN, as somatosensory corticopontine projections in *Nex-cKO* mice are changed to resemble motor-like projections. Cb, cerebellum; CP, cerebral peduncle; SC, spinal cord.

region allocated to motor axons. This strongly suggests that, during the establishment of corticopontine topography, both structures – the neocortex and the pons – need to be properly pre-patterned by factors involved in spatial and temporal control of neurogenesis, such as *Nr2f1* for the cortex and *Hoxa5* for the pontine nuclei (model in Fig. 8).

Conclusions and outlook

By showing that gradient cortical expression of the transcriptional regulator Nr2f1 is directly involved in the establishment of corticopontine topographic mapping, we provide new insights into the development of neural systems. However, other factors regulating the size and location of cortical areas are also likely implicated. We conclude that distinct molecular mechanisms in the source (cerebral cortex) and target (pontine nuclei) regions must be coordinated during the establishment of corticopontine topography. Identifying the molecular pathways within the cortex and pontine nuclei, as well as the mechanisms and molecules governing their interaction remains an open question for further studies.

Limitations of the study

This study shows a limited number of viral injections per cortical area that was partially compensated by adapting mouse tract-tracing data from the Allen Brain Institute to our analysis. Even though both groups of samples showed a highly consistent pattern of topographical organization, the two types of data resulted from different experimental conditions. Because of some variability of the fluorescent signal among samples, we chose to focus on 3D spatial distribution patterns that turned out to be consistent across all control experiments. We found the *Emx1-cKO* mouse model less suitable for further topographical analysis due to the disorganized and chaotic innervation pattern observed in the *Thy1*-e*YFP-H* reporter background. Although more sophisticated methods are needed to pinpoint the cellular and molecular mechanisms involved in the establishment of corticofugal topography, our study represents a useful starting point and resource for further studies of the development of corticopontine and corticospinal projections in mice.

MATERIALS AND METHODS

Topographical map of corticopontine projections from somatosensory and motor areas

To establish a 3D benchmark map of corticopontine projections from somatosensory and motor areas in adult wild-type mice, we used a selection of public experimental tract-tracing data available from the Allen Institute mouse brain connectivity atlas (http://connectivity.brain-map.org/). We selected 11 experiments in which the anterograde tracer EGFP was injected in the right primary/secondary motor cortex (n=6) or primary somatosensory cortex (n=5) of wild-type C57BL/6J mice (Table S1). Serial two-photon fluorescence images were interactively inspected using the Projection High Resolution Image viewer of the Allen Institute and, from each case, five sagittally oriented images of the right pontine nuclei spaced at ∼100 µm were captured by screen shot from the largest 3D multiplane thumbnail viewer. The resolution of the captured images was up-sampled to three times the original size before their spatial alignment to the CCFv3 was optimized using the tools QuickNII (Puchades et al., 2019) and VisuAlign (RRID: SCR_017978), as described below. These images were used to create 3D representations of the axonal labelling in the pontine nuclei (Fig. 2; see below).

Animals

All mice used were bred in a C57BL/6J background. Male and female animals at any stage of development were used. All experiments were conducted in accordance with the French Animal Welfare Act and European guidelines for the use of experimental animals, using protocols approved by the French Ministry of Education, Research and Innovation and the local ethics committee (CIEPAL NCE/2019–548, Nice) under authorization #15 349 and #15 350. *Nr2f1* mice were crossed with *Emx1-Cre-recombinase* mice to inactivate *Nr2f1* exclusively in cortical progenitors and their progeny (Armentano et al., 2007) or with *Nex-Cre-recombinase* mice to abolish *Nr2f1* expression from postmitotic neurons (Alfano et al., 2014). Littermate *Nr2f1* mice without the presence of the *Cre-recombinase* gene (*Cre-negatives*) were considered controls (Table S2). For postnatal day (P)

Development (2022) 149, dev200026. doi:10.1242/dev.200026

21 and adult topographic map analysis, *Emx1-cKO* and *Nex-cKO* animals were further crossed with *Thy1-eYFP-H* mice to specifically label layer V projection neurons, as previously reported (Harb et al., 2016; Porrero et al., 2010). Mice were genotyped as previously described (Alfano et al., 2014; Armentano et al., 2007; Harb et al., 2016). Control and mutant littermates were genotyped as *Nr2f1*$^{fl/fl}$*:Thy1-eYFP-H*$^{T/+}$ (control) and *Nr2f1*$^{fl/fl}$*:Emx1-Cre:Thy1-eYFP-H*$^{T/+}$ (mutant) or *Nr2f1*$^{fl/fl}$*:Nex-Cre:Thy1-eYFP-H*$^{T/+}$ (mutant). For simplicity, mutant mice are named *Emx1-cKO* and *Nex-cKO* throughout the text. Midday of the day of the observed vaginal plug was considered as embryonic day (E) 0.5.

Anterograde tracing of corticospinal axons in early postnatal mice

P4-P5 animals were anesthetized on ice for 5 min and kept on ice during the whole procedure. Viral particles were produced from the AAV9-CAGtdTomato plasmid by Alexis Bemelmans (CEA, France) and diluted 1:50 in TE-Buffer (Qiagen, 1018499) to a final concentration of 1.75e12 vg/ml (kindly donated by I. Dusart, Pierre and Marie Curie University, Paris, France). Approximately 0.5/1 µl was injected unilaterally in different rostral-caudal and medio-lateral brain locations of control and *Nex-cKO* pups, as previously described (Gu et al., 2017).

Microscopic imaging

Mosaic microscopic images were acquired using an Axio Imager M2 epifluorescence microscope (Zeiss) equipped with a halogen lamp, a MCU 2008 motorized stage and an EC Plan-Neofluar 10×/0.30 (Figs 3A-D,B′-D′, 4B-D,B′-D′, 5B-L, 6B′,C′, 7B′-C′; Figs S1, S2; S3 columns 3 and 4, S4 columns 3 and 4) or an EC Plan-Neofluar 2.5×/0.075 (Figs 6B-C, 7B-C; Figs S3 column 2, S4 column 2) and an AxioCam MRm camera. ZEN blue software was used for imaging and automatic stitching. Images were exported in TIFF format and serially ordered from lateral to medial, rotated and, if needed, mirrored to consistent anatomical orientation using Adobe Photoshop CS6 (RRID: SCR_014199), before being converted to PNG format and resized to 60% of original size using ImageJ (RRID: SCR_003070) with bilinear interpolation. The resized serial images were loaded into Adobe Photoshop as a stack, spatially aligned using the ventral surfaces of the pons and cerebral peduncle as landmarks, and cropped and exported as individual PNG files. For comparative analyses of topographical organization (see below), variations in YFP signal expression intensity within and between groups were normalized by adjusting the brightness and contrast of images to equal levels using a custom-made histogram matching script available for ImageJ (National Institutes of Health; https://imagej.nih.gov/). One selected, a representative case (Experiment 5, Cre-negative, nr: 14250, Table S2) was used as reference.

Spatial alignment to common 3D reference atlas

Serial sectional images were spatially registered to the *Allen Mouse Common Coordinate Framework*, version 3, 2017 edition of the delineations (CCFv3; Wang et al., 2020) using the QuickNII software tool (RRID:SCR_016854; Puchades et al., 2019). Multiple anatomical landmarks (hippocampus, caudate-putamen, inferior and superior colliculus, and the external surface of the neocortex) were used to determine the medio-lateral position and orientation of the sagittal section images. For each section image, custom atlas diagrams were aligned to anatomical landmarks in the experimental images using affine transformations, with emphasis on matching the ventral surface of the pons and white matter tracts close to the pontine nuclei and exported as PNG images. As a secondary step, to further optimize registration, the custom atlas images were non-linearly transformed using the software tool VisuAlign v0.8 (RRID:SCR_017978), with particular focus on fitting the template to the outer brain surface, subcortical white matter and the outer boundaries of the pontine nuclei. To co-display images and the spatially registered custom atlas images, we used the software tool LocaliZoom, which is embedded in the Navigator3 image management system (bit.ly/navigator3), developed and hosted by the Neural Systems Laboratory at the University of Oslo, Norway.

Cortical distribution analysis in *Emx1-cKO* and *Nex-cKO* mutants

Serial section images from *Nex-cKO* and *Emx1-cKO* mutants co-registered to the *Allen Mouse Brain Connectivity Atlas* were analysed using an ImageJ macro allowing automatic counting of spots by area of interest in the brain. The spots are considered as specific staining using a threshold based on intensity and shape of the elements, and the composite RGB segmentation atlas is used as a mask for the region of interest. The macro pre-processes an atlas plate to delineate the regions of interest (ROI), based upon their unique colour-code and corrects the corresponding raw image by subtracting the background, generating binary images of the signal and combining these to the ROI maps. Finally, all objects within circularity range of 0.5-1 were counted per ROI using the 'find maxima' tool. The process, reiterated for each atlas plate-raw image combination, produced a summary table containing the quantification of particles per area per section, shown as graphs in Fig. 3.

Corticospinal tract morphometric analysis in *Emx1-cKO* and *Nex-cKO* mutants

Serial section images from *Nex-cKO* and *Emx1-cKO* mutants were analysed using the Fiji-ImageJ Software tool (Schindelin et al., 2015) to determine the total dorsoventral width of the bundle expressing fluorescent signal in the descending fibre tract in different positions: rostrally and caudally to the pontine nuclei; and 250 µm and 500 µm caudal to the nuclei. The width of separate fibre fascicles was also measured 250 µm and 500 µm from the terminal edge of the pontine nuclei (Fig. 4A′).

Analysis of tracer injection sites

Serial section images of cortical tracer injections in *Nex-cKO* brains (Table S3) and experiments taken from the Allen Mouse Brain Connectivity Atlas, were spatially aligned using QuickNII and VisuAlign, as described above. The centre positions of the injection sites were annotated as a point-coordinate using LocaliZoom and co-displayed with the CCFv3 atlas in the 3D viewer tool MeshView (RRID:SCR_017222). These visualizations were used to select spatially corresponding injection site locations for analyses of spatial distribution of corticopontine projections.

Histology, immunohistochemistry and *in situ* hybridization

At P21 and adulthood, animals were anesthetized by intraperitoneal injection of a mixture of Tiletamine-Zolazepam-Xylazine-Buprenorphine and intracardially perfused with phosphate-buffered saline (PBS) followed by 4% paraformaldehyde (PFA) in PBS. Specifically, 15 ml of PBS was used for both P21 and adult animals, followed by 20 or 30 ml of PFA for P21 and adults, respectively, and according to the average body weight of the animals. Brains were removed from the skull and postfixed for 4 h at 4°C in 4% PFA, before being vibratome sagittally sectioned at 100 µm (adult samples) or 150 µm (P21 samples). All sections were incubated overnight at 4°C in a solution of 0.5% Triton X-100, 3% BSA, 10% goat serum in PBS, for permeabilization and reduction of non-specific binding of antibodies. For immunofluorescence (IF), sections were incubated for 2 days at 4°C with primary antibodies in a solution of 0.5% Triton X-100, 10% goat serum in PBS and then overnight at 4°C with relative secondary antibodies and Hoechst diluted in PBS. For the complete list of primary and secondary antibodies, see Table S5. Sections were washed several times in PBS, then transferred on Superfrost plus slides (ThermoScientific), covered and dried for 30 min to 1 h, and finally mounted with the Mowiol (Sigma-Aldrich) mounting medium.

Semi-quantitative recording and 3D visualization of spatial distribution patterns

To investigate and compare the 3D distributions of YFP signal expression or anterograde axonal labelling within the pontine nuclei, we used the annotation functionality in the LocaliZoom tool to semi-quantitatively record YFP signal expression or labelled axons in all sections through the pontine nuclei as point coordinates (specified in the coordinate system of the reference atlas, CCFv3), reflecting the overall density of signal/labelling observed in the images (Fig. 2C,D). To compensate for the spacing between sections and allow inspection of point distributions perpendicularly to the section angle, the *z*-coordinate of each point was randomly displaced within the thickness of the gap between sections using a custom Python script. The point coordinates were co-displayed in the MeshView 3D viewer tool (Figs 2, 5, 6 and 7).

Acknowledgements
We thank Isabelle Dusart in Paris for providing us with AAV9-CAG-tdTomato viral particles produced by Alexis Bemelmans (CEA, France); Nicolaas Groeneboom and Gergely Csucs for expert technical assistance; Baptiste Monterroso and Sameh Ben Aicha of the iBV PRISM microscopy platform for the set-up and optimization of automatic image analysis tools used in this work; and Sharon Yates and Maja A. Puchades for useful discussions.

Competing interests
The authors declare no competing or financial interests.

Author contributions
Conceptualization: C.T., M.Ø., J.G.B., T.B.L., M.S.; Methodology: C.T., M.Ø., J.G.B., T.B.L., M.S.; Software: J.G.B.; Validation: C.T., M.Ø., J.G.B., T.B.L., M.S.; Formal analysis: C.T., M.Ø., J.G.B., T.B.L., M.S.; Investigation: C.T., M.Ø., T.B.L., M.S.; Resources: J.G.B., T.B.L., M.S.; Data curation: C.T., M.Ø., T.B.L., M.S.; Writing - original draft: M.S.; Writing - review & editing: C.T., M.Ø., J.G.B., T.B.L.; Visualization: C.T., M.Ø., T.B.L., M.S.; Supervision: T.B.L., M.S.; Project administration: M.S.; Funding acquisition: C.T., J.G.B., T.B.L., M.S.

Funding
This work was funded by the Fondation Recherche Médicale (Equipe FRM 2015 DEQ20150331750 to M.S.), by the French Government (National Research Agency, ANR) through the 'Investments for the Future' programs LABEX SIGNALIFE ANR-11-LABX-0028-01 and IDEX UCAJedi ANR-15-IDEX-01 to M.S., by a PhD contract from Région PACA/Inserm and Fondation Recherche Médicale (FDT201904008137 to C.T.), by the European Union Horizon 2020 Framework Program for Research and Innovation (945539 Human Brain Project SGA3 to J.G.B. and T.B.L.), and by The Research Council of Norway (Norges forskningsråd; 269774 INCF Norwegian Node to J.G.B. and T.B.L.). Open access funding provided by the University of Oslo. Deposited in PMC for immediate release.

Data availability
Microscopic images are available via the EBRAINS research infrastructure (https://search.kg.ebrains.eu/) as high-resolution TIFF images under a CC-BY 4.0 licence, as two data sets entitled: (1) Impact of area patterning genes on corticopontine projection topography: Microscopic visualization of genetically controlled yellow fluorescence protein expression in Nr2f1 conditional knockout mice lacking progenitor or postmitotic expression of Nr2f1 (https://doi.org/10.25493/RYZ4-DB9); and (2) Impact of area patterning genes on corticopontine projection topography: Anterograde tracing of corticopontine projections in Nr2f1 conditional knockout mice lacking postmitotic expression of Nr2f1 (https://doi.org/10.25493/RNK8-CAN). The custom Python script (spread.py) used is available from GitHub (https://github.com/Neural-Systems-at-UIO/nutil/blob/master/scripts/spread.py). The QuickNII (v2.2, RRID: SCR_016854; Puchades et al., 2019) LocaliZoom and Meshview (RRID: SCR_0170222) softwares are available from EBRAINS (https://search.kg.ebrains.eu/).

Peer review history
The peer review history is available online at https://journals.biologists.com/dev/article-lookup/doi/10.1242/dev.200026.

References

Alfano, C. and Studer, M. (2012). Neocortical arealization: evolution, mechanisms and open questions. *Dev. Neurobiol.* **73**, 411-447. doi:10.1002/dneu.22067
Alfano, C., Magrinelli, E., Harb, K., Hevner, R. F. and Studer, M. (2014). Postmitotic control of sensory area specification during neocortical development. *Nat. Commun.* **5**, 5632. doi:10.1038/ncomms6632
Altman, J. and Bayer, S. A. (1987). Development of the precerebellar nuclei in the rat: IV. The anterior precerebellar extramural migratory stream and the nucleus reticularis tegmenti pontis and the basal pontine gray. *J. Comp. Neurol.* **257**, 529-552. doi:10.1002/cne.902570405
Armentano, M., Chou, S.-J., Tomassy, G. S., Leingartner, A., O'Leary, D. D. and Studer, M. (2007). COUP-TFI regulates the balance of cortical patterning between frontal/motor and sensory areas. *Nat. Neurosci.* **10**, 1277-1286. doi:10.1038/nn1958
Assimacopoulos, S., Kao, T., Issa, N. P. and Grove, E. A. (2012). Fibroblast growth factor 8 organizes the neocortical area map and regulates sensory map topography. *J. Neurosci.* **32**, 7191-7201. doi:10.1523/JNEUROSCI.0071-12.2012
Badura, A., Schonewille, M., Voges, K., Galliano, E., Renier, N., Gao, Z., Witter, L., Hoebeek, F. E., Chédotal, A. and De Zeeuw, C. I. (2013). Climbing fiber input shapes reciprocity of Purkinje cell firing. *Neuron* **78**, 700-713. doi:10.1016/j.neuron.2013.03.018
Bertacchi, M., Parisot, J. and Studer, M. (2019). The pleiotropic transcriptional regulator COUP-TFI plays multiple roles in neural development and disease. *Brain Res.* **1705**, 75-94. doi:10.1016/j.brainres.2018.04.024
Bjaalie, J. G. and Brodal, P. (1989). Visual pathways to the cerebellum: segregation in the pontine nuclei of terminal fields from different visual cortical areas in the cat. *Neuroscience* **29**, 95-107. doi:10.1016/0306-4522(89)90335-7
Bjaalie, J. G. and Brodal, P. (1997). Cat pontocerebellar network: numerical capacity and axonal collateral branching of neurones in the pontine nuclei projecting to individual paraflocculus folia. *Neurosci. Res.* **27**, 199-210. doi:10.1016/S0168-0102(96)01149-2
Bower, J. M. (2011). Functional implications of tactile projection patterns to the lateral hemispheres of the cerebellum of the albino rat: the legacy of Wally Welker. *Ann. N. Y. Acad. Sci.* **1225**, 130-141. doi:10.1111/j.1749-6632.2011.06020.x
Bower, J. M. and Kassel, J. (1990). Variability in tactile projection patterns to cerebellar folia crus IIA of the Norway rat. *J. Comp. Neurol.* **302**, 768-778. doi:10.1002/cne.903020409
Bower, J. M., Beermann, D. H., Gibson, J. M., Shambes, G. M. and Welker, W. (1981). Principles of organization of a cerebro-cerebellar circuit. Micromapping the projections from cerebral (SI) to cerebellar (granule cell layer) tactile areas of rats. *Brain Behav. Evol.* **18**, 1-18. doi:10.1159/000121772
Brodal, P. (1978). The corticopontine projection in the rhesus monkey. Origin and principles of organization. *Brain* **101**, 251-283. doi:10.1093/brain/101.2.251
Brodal, P. and Bjaalie, J. G. (1992). Organization of the pontine nuclei. *Neurosci. Res.* **13**, 83-118. doi:10.1016/0168-0102(92)90092-Q
Buckner, R. L. (2013). The cerebellum and cognitive function: 25 years of insight from anatomy and neuroimaging. *Neuron* **80**, 807-815. doi:10.1016/j.neuron.2013.10.044
Cadwell, C. R., Bhaduri, A., Mostajo-Radji, M. A., Keefe, M. G. and Nowakowski, T. J. (2019). Development and arealization of the cerebral cortex. *Neuron* **103**, 980-1004. doi:10.1016/j.neuron.2019.07.009
Cederquist, G. Y., Azim, E., Shnider, S. J., Padmanabhan, H. and Macklis, J. D. (2013). Lmo4 establishes rostral motor cortex projection neuron subtype diversity. *J. Neurosci.* **33**, 6321-6332. doi:10.1523/JNEUROSCI.5140-12.2013
Chapin, J. K. and Lin, C. S. (1984). Mapping the body representation in the SI cortex of anesthetized and awake rats. *J. Comp. Neurol.* **229**, 199-213. doi:10.1002/cne.902290206
D'Elia, K. P. and Dasen, J. S. (2018). Topographic maps: motor axons wait their turn. *Curr. Biol.* **28**, R86-R88. doi:10.1016/j.cub.2017.11.047
Erzurumlu, R. S., Murakami, Y. and Rijli, F. M. (2010). Mapping the face in the somatosensory brainstem. *Nat. Rev. Neurosci.* **11**, 252-263. doi:10.1038/nrn2804
Fabri, M. and Burton, H. (1991). Ipsilateral cortical connections of primary somatic sensory cortex in rats. *J. Comp. Neurol.* **311**, 405-424. doi:10.1002/cne.903110310
Feng, G., Mellor, R. H., Bernstein, M., Keller-Peck, C., Nguyen, Q. T., Wallace, M., Nerbonne, J. M., Lichtman, J. W. and Sanes, J. R. (2000). Imaging neuronal subsets in transgenic mice expressing multiple spectral variants of GFP. *Neuron* **28**, 41-51. doi:10.1016/S0896-6273(00)00084-2
Flore, G., Di Ruberto, G., Parisot, J., Sannino, S., Russo, F., Illingworth, E. A., Studer, M. and De Leonibus, E. (2017). Gradient COUP-TFI expression is required for functional organization of the hippocampal septo-temporal longitudinal axis. *Cereb. Cortex* **27**, 1629-1643. doi:10.1093/cercor/bhv336
Fritzsch, B., Elliott, K. L. and Pavlinkova, G. (2019). Primary sensory map formations reflect unique needs and molecular cues specific to each sensory system. *F1000Res* **8**, 345. doi:10.12688/f1000research.17717.1
Goebbels, S., Bormuth, I., Bode, U., Hermanson, O., Schwab, M. H. and Nave, K. A. (2006). Genetic targeting of principal neurons in neocortex and hippocampus of NEX-Cre mice. *Genesis* **44**, 611-621. doi:10.1002/dvg.20256
Greig, L. C., Woodworth, M. B., Galazo, M. J., Padmanabhan, H. and Macklis, J. D. (2013). Molecular logic of neocortical projection neuron specification, development and diversity. *Nat. Rev. Neurosci.* **14**, 755-769. doi:10.1038/nrn3586
Gu, Z., Kalambogias, J., Yoshioka, S., Han, W., Li, Z., Kawasawa, Y. I., Pochareddy, S., Li, Z., Liu, F., Xu, X. et al. (2017). Control of species-dependent cortico-motoneuronal connections underlying manual dexterity. *Science* **357**, 400-404. doi:10.1126/science.aan3721
Harb, K., Magrinelli, E., Nicolas, C. S., Lukianets, N., Frangeul, L., Pietri, M., Sun, T., Sandoz, G., Grammont, F., Jabaudon, D. et al. (2016). Area-specific development of distinct projection neuron subclasses is regulated by postnatal epigenetic modifications. *eLife* **5**, e09531. doi:10.7554/eLife.09531
Heffner, C. D., Lumsden, A. G. and O'Leary, D. D. (1990). Target control of collateral extension and directional axon growth in the mammalian brain. *Science* **247**, 217-220. doi:10.1126/science.2294603
Henschke, J. U. and Pakan, J. M. (2020). Disynaptic cerebrocerebellar pathways originating from multiple functionally distinct cortical areas. *eLife* **9**, e59148. doi:10.7554/eLife.59148.sa2
Inoue, K., Terashima, T. and Inoue, Y. (1991). Postnatal development of the pontine projections from the visual cortex of the mouse. *Okajimas Folia Anat. Jpn.* **67**, 479-492. doi:10.2535/ofaj1936.67.6_479

Leergaard, T. B. (2003). Clustered and laminar topographic patterns in rat cerebropontine pathways. *Anat Embryol (Berl)* **206**, 149-162. doi:10.1007/s00429-002-0272-7
Leergaard, T. B. and Bjaalie, J. G. (2007). Topography of the complete corticopontine projection: from experiments to principal Maps. *Front Neurosci* **1**, 211-223. doi:10.3389/neuro.01.1.1.016.2007
Leergaard, T. B., Lakke, E. A. and Bjaalie, J. G. (1995). Topographical organization in the early postnatal corticopontine projection: a carbocyanine dye and 3-D computer reconstruction study in the rat. *J. Comp. Neurol.* **361**, 77-94. doi:10.1002/cne.903610107
Leergaard, T. B., Alloway, K. D., Mutic, J. J. and Bjaalie, J. G. (2000a). Three-dimensional topography of corticopontine projections from rat barrel cortex: correlations with corticostriatal organization. *J. Neurosci.* **20**, 8474-8484. doi:10.1523/JNEUROSCI.20-22-08474.2000
Leergaard, T. B., Lyngstad, K. A., Thompson, J. H., Taeymans, S., Vos, B. P., De Schutter, E., Bower, J. M. and Bjaalie, J. G. (2000b). Rat somatosensory cerebropontocerebellar pathways: spatial relationships of the somatotopic map of the primary somatosensory cortex are preserved in a three-dimensional clustered pontine map. *J. Comp. Neurol.* **422**, 246-266. doi:10.1002/(SICI)1096-9861(20000626)422:2<246::AID-CNE7>3.0.CO;2-R
Leergaard, T. B., Alloway, K. D., Pham, T. A., Bolstad, I., Hoffer, Z. S., Pettersen, C. and Bjaalie, J. G. (2004). Three-dimensional topography of corticopontine projections from rat sensorimotor cortex: comparisons with corticostriatal projections reveal diverse integrative organization. *J. Comp. Neurol.* **478**, 306-322. doi:10.1002/cne.20289
Leergaard, T. B., Lillehaug, S., De Schutter, E., Bower, J. M. and Bjaalie, J. G. (2006). Topographical organization of pathways from somatosensory cortex through the pontine nuclei to tactile regions of the rat cerebellar hemispheres. *Eur. J. Neurosci.* **24**, 2801-2812. doi:10.1111/j.1460-9568.2006.05150.x
Lemon, R. N. (2008). Descending pathways in motor control. *Annu. Rev. Neurosci.* **31**, 195-218. doi:10.1146/annurev.neuro.31.060407.125547
Liu, Q., Dwyer, N. D. and O'Leary, D. D. (2000). Differential expression of COUP-TFI, CHL1, and two novel genes in developing neocortex identified by differential display PCR. *J. Neurosci.* **20**, 7682-7690. doi:10.1523/JNEUROSCI.20-20-07682.2000
Maheshwari, U., Kraus, D., Vilain, N., Holwerda, S. J. B., Cankovic, V., Maiorano, N. A., Kohler, H., Satoh, D., Sigrist, M., Arber, S. et al. (2020). Postmitotic hoxa5 expression specifies pontine neuron positional identity and input connectivity of cortical afferent subsets. *Cell Reports* **31**, 107767. doi:10.1016/j.celrep.2020.107767
McLaughlin, T. and O'Leary, D. D. M. (2005). Molecular gradients and development of retinotopic maps. *Annu. Rev. Neurosci.* **28**, 327-355. doi:10.1146/annurev.neuro.28.061604.135714
Mihailoff, G. A., Lee, H., Watt, C. B. and Yates, R. (1985). Projections to the basilar pontine nuclei from face sensory and motor regions of the cerebral cortex in the rat. *J. Comp. Neurol.* **237**, 251-263. doi:10.1002/cne.902370209
Mottolese, C., Richard, N., Harquel, S., Szathmari, A., Sirigu, A. and Desmurget, M. (2013). Mapping motor representations in the human cerebellum. *Brain* **136**, 330-342. doi:10.1093/brain/aws186
Nitschke, M. F., Kleinschmidt, A., Wessel, K. and Frahm, J. (1996). Somatotopic motor representation in the human anterior cerebellum. A high-resolution functional MRI study. *Brain* **119**, 1023-1029. doi:10.1093/brain/119.3.1023
O'Leary, D. D. and Sahara, S. (2008). Genetic regulation of arealization of the neocortex. *Curr. Opin. Neurobiol.* **18**, 90-100. doi:10.1016/j.conb.2008.05.011
O'Leary, D. D. and Terashima, T. (1988). Cortical axons branch to multiple subcortical targets by interstitial axon budding: implications for target recognition and "waiting periods". *Neuron* **1**, 901-910. doi:10.1016/0896-6273(88)90147-X
Peterburs, J. and Desmond, J. E. (2016). The role of the human cerebellum in performance monitoring. *Curr. Opin. Neurobiol.* **40**, 38-44. doi:10.1016/j.conb.2016.06.011
Petersen, S. C., Watson, J. D., Richmond, J. E., Sarov, M., Walthall, W. W. and Miller, D. M.III (2011). A transcriptional program promotes remodeling of GABAergic synapses in Caenorhabditis elegans. *J. Neurosci.* **31**, 15362-15375. doi:10.1523/JNEUROSCI.3181-11.2011
Polleux, F., Dehay, C. and Kennedy, H. (1997). The timetable of laminar neurogenesis contributes to the specification of cortical areas in mouse isocortex. *J. Comp. Neurol.* **385**, 95-116. doi:10.1002/(SICI)1096-9861(19970818)385:1<95::AID-CNE6>3.0.CO;2-7
Porrero, C., Rubio-Garrido, P., Avendano, C. and Clasca, F. (2010). Mapping of fluorescent protein-expressing neurons and axon pathways in adult and developing Thy1-eYFP-H transgenic mice. *Brain Res.* **1345**, 59-72. doi:10.1016/j.brainres.2010.05.061
Pourchet, O., Morel, M. P., Welniarz, Q., Sarrazin, N., Marti, F., Heck, N., Gallea, C., Doulazmi, M., Roig Puiggros, S., Moreno-Bravo, J. A. et al. (2021). Loss of floor plate Netrin-1 impairs midline crossing of corticospinal axons and leads to mirror movements. *Cell Reports* **34**, 108654. doi:10.1016/j.celrep.2020.108654
Proville, R. D., Spolidoro, M., Guyon, N., Dugue, G. P., Selimi, F., Isope, P., Popa, D. and Lena, C. (2014). Cerebellum involvement in cortical sensorimotor circuits for the control of voluntary movements. *Nat. Neurosci.* **17**, 1233-1239. doi:10.1038/nn.3773
Puchades, M. A., Csucs, G., Ledergerber, D., Leergaard, T. B. and Bjaalie, J. G. (2019). Spatial registration of serial microscopic brain images to three-dimensional reference atlases with the QuickNII tool. *PLoS ONE* **14**, e0216796. doi:10.1371/journal.pone.0216796
Schindelin, J., Rueden, C. T., Hiner, M. C. and Eliceiri, K. W. (2015). The ImageJ ecosystem: an open platform for biomedical image analysis. *Mol. Reprod. Dev.* **82**, 518-529. doi:10.1002/mrd.22489
Schmahmann, J. D. and Pandya, D. N. (1997). Anatomic organization of the basilar pontine projections from prefrontal cortices in rhesus monkey. *J. Neurosci.* **17**, 438-458. doi:10.1523/JNEUROSCI.17-01-00438.1997
Shambes, G. M., Gibson, J. M. and Welker, W. (1978). Fractured somatotopy in granule cell tactile areas of rat cerebellar hemispheres revealed by micromapping. *Brain Behav. Evol.* **15**, 94-140. doi:10.1159/000123774
Shepherd, G. M. (2009). Intracortical cartography in an agranular area. *Front. Neurosci.* **3**, 337-343. doi:10.3389/neuro.01.030.2009
Smart, I. H. (1984). Histogenesis of the mesocortical area of the mouse telencephalon. *J. Anat.* **138**, 537-552.
Stoodley, C. J. and Schmahmann, J. D. (2010). Evidence for topographic organization in the cerebellum of motor control versus cognitive and affective processing. *Cortex* **46**, 831-844. doi:10.1016/j.cortex.2009.11.008
Tomasch, J. (1968). The overall information carrying capacity of the major afferent and efferent cerebellar cell and fiber systems. *Confin Neurol* **30**, 359-367. doi:10.1159/000103549
Tomasch, J. (1969). The numerical capacity of the human cortico-pontocerebellar system. *Brain Res.* **13**, 476-484. doi:10.1016/0006-8993(69)90261-3
Tomassy, G. S., De Leonibus, E., Jabaudon, D., Lodato, S., Alfano, C., Mele, A., Macklis, J. D. and Studer, M. (2010). Area-specific temporal control of corticospinal motor neuron differentiation by COUP-TFI. *Proc. Natl. Acad. Sci. USA* **107**, 3576-3581. doi:10.1073/pnas.0911792107
Wang, Q., Ding, S. L., Li, Y., Royall, J., Feng, D., Lesnar, P., Graddis, N., Naeemi, M., Facer, B., Ho, A. et al. (2020). The Allen mouse brain common coordinate framework: a 3D reference atlas. *Cell* **181**, 936-953. doi:10.1016/j.cell.2020.04.007
Welker, C. (1971). Microelectrode delineation of fine grain somatotopic organization of (SmI) cerebral neocortex in albino rat. *Brain Res.* **26**, 259-275. doi:10.1016/S0006-8993(71)80004-5
Woolsey, T. A. and Van der Loos, H. (1970). The structural organization of layer IV in the somatosensory region (SI) of mouse cerebral cortex. The description of a cortical field composed of discrete cytoarchitectonic units. *Brain Res.* **17**, 205-242. doi:10.1016/0006-8993(70)90079-X
Zhou, H. M. and Walthall, W. W. (1998). UNC-55, an orphan nuclear hormone receptor, orchestrates synaptic specificity among two classes of motor neurons in Caenorhabditis elegans. *J. Neurosci.* **18**, 10438-10444. doi:10.1523/JNEUROSCI.18-24-10438.1998
Zhou, C., Tsai, S. Y. and Tsai, M.-J. (2001). COUP-TFI: an intrinsic factor for early regionalization of the neocortex. *Genes Dev.* **15**, 2054-2059. doi:10.1101/gad.913601

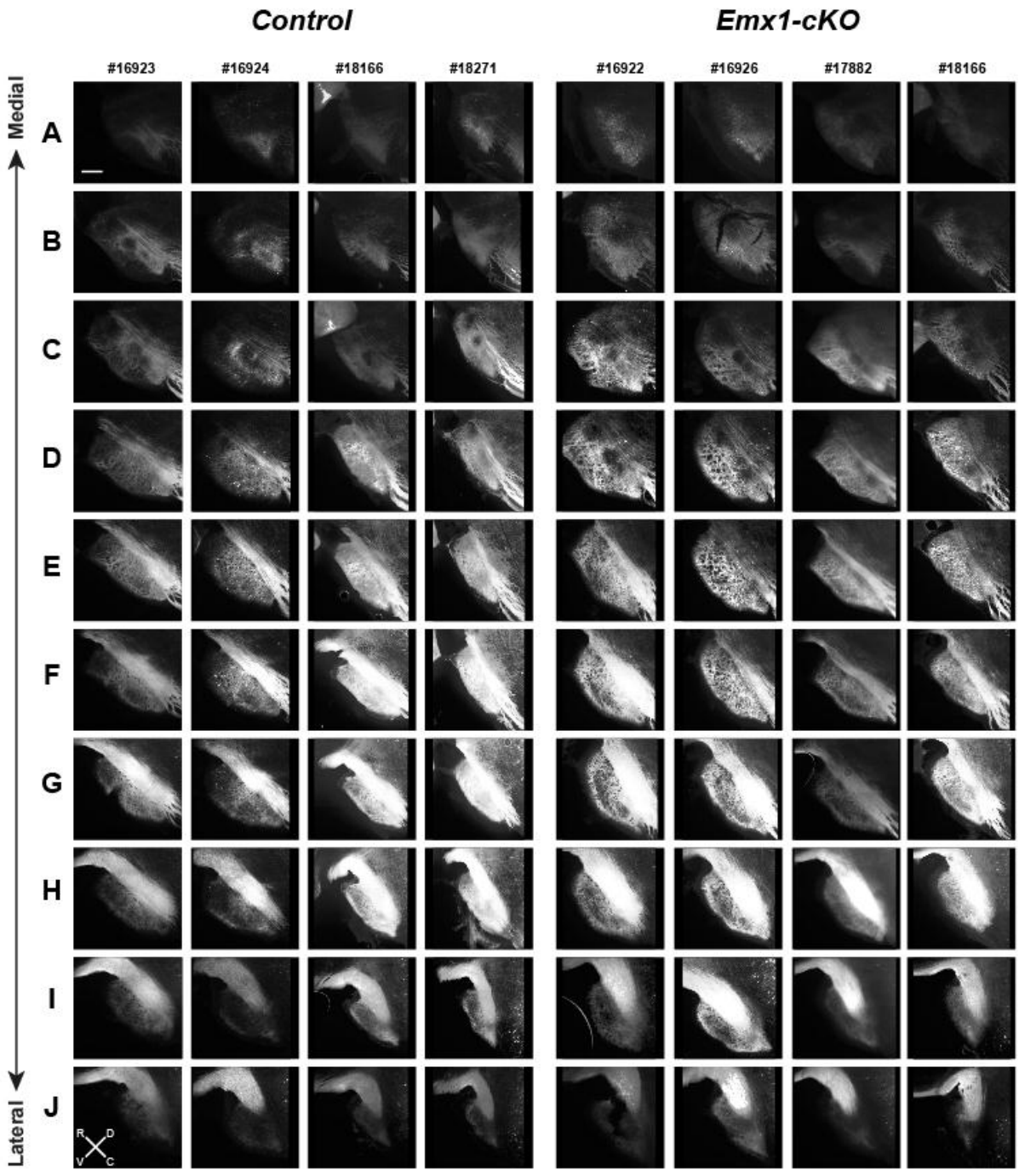

Fig. S1. Overview of YFP-expression in *Emx1-cKO* mice and controls

Fluorescence microscopy images of the pontine nuclei in sagittal sections from 4 control and 4 *Emx1-cKO* mice. Columns show images from one animal, with sections from corresponding levels from medial to lateral sorted from top to bottom (rows A-J). The intensity levels of the images have been normalized. Signal expression in *Emx1-cKO* mice is more widespread and more diffusely distributed in the pontine nuclei, relative to controls. Scale bar, 200µm.

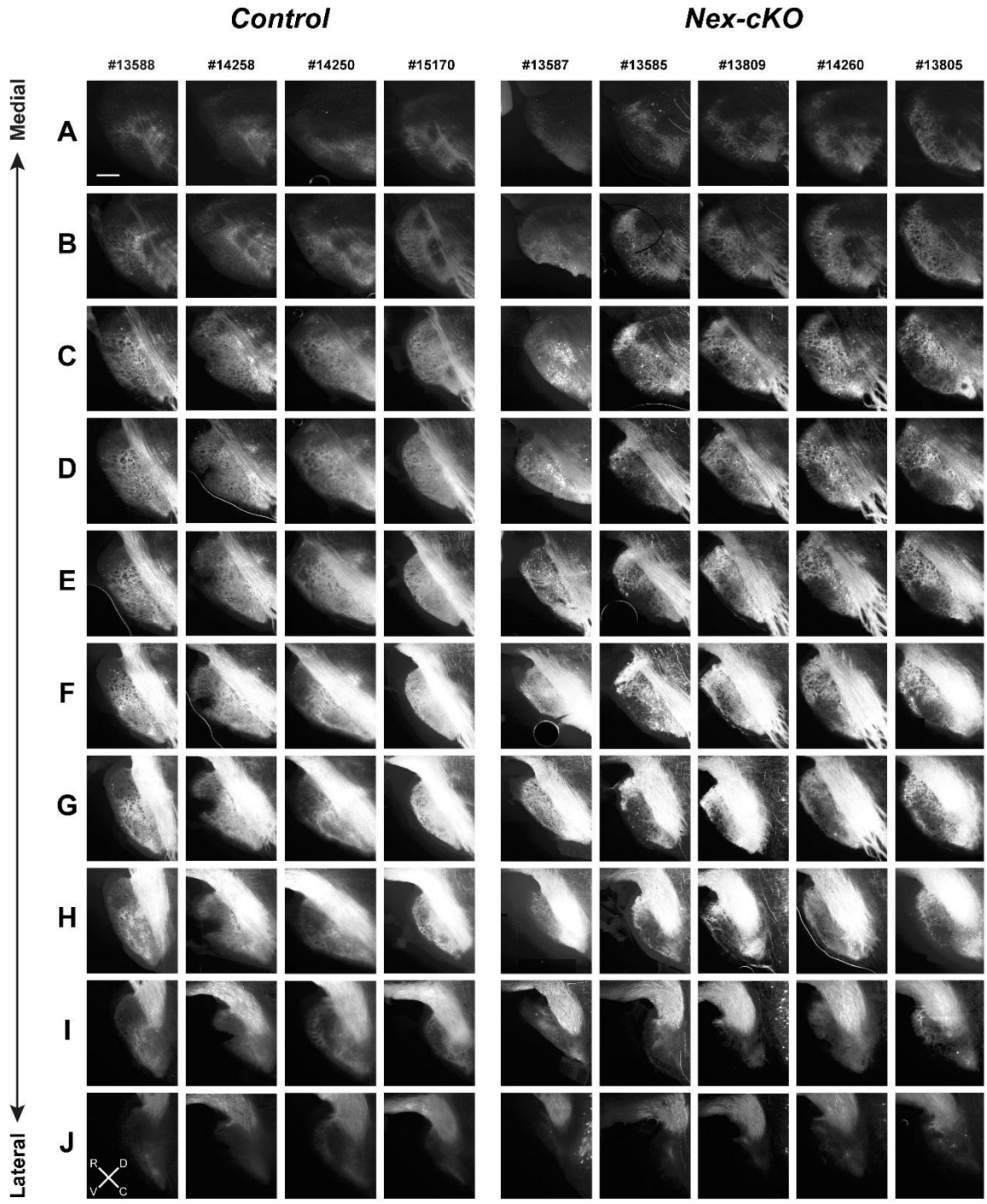

Fig. S2. Overview of YFP-expression in *Nex-cKO* mice and controls

Fluorescence microscopy images of the pontine nuclei in sagittal sections from 4 control and 4 *Nex-cKO* mice. Columns show images from one animal, with sections from corresponding levels from medial to lateral sorted from top to bottom (rows A-J). The intensity levels of the images have been normalized. Signal expression in *Nex-cKO* mice is reduced or absent in the central core region of the pontine nuclei, relative to controls. Scale bar, 200µm.

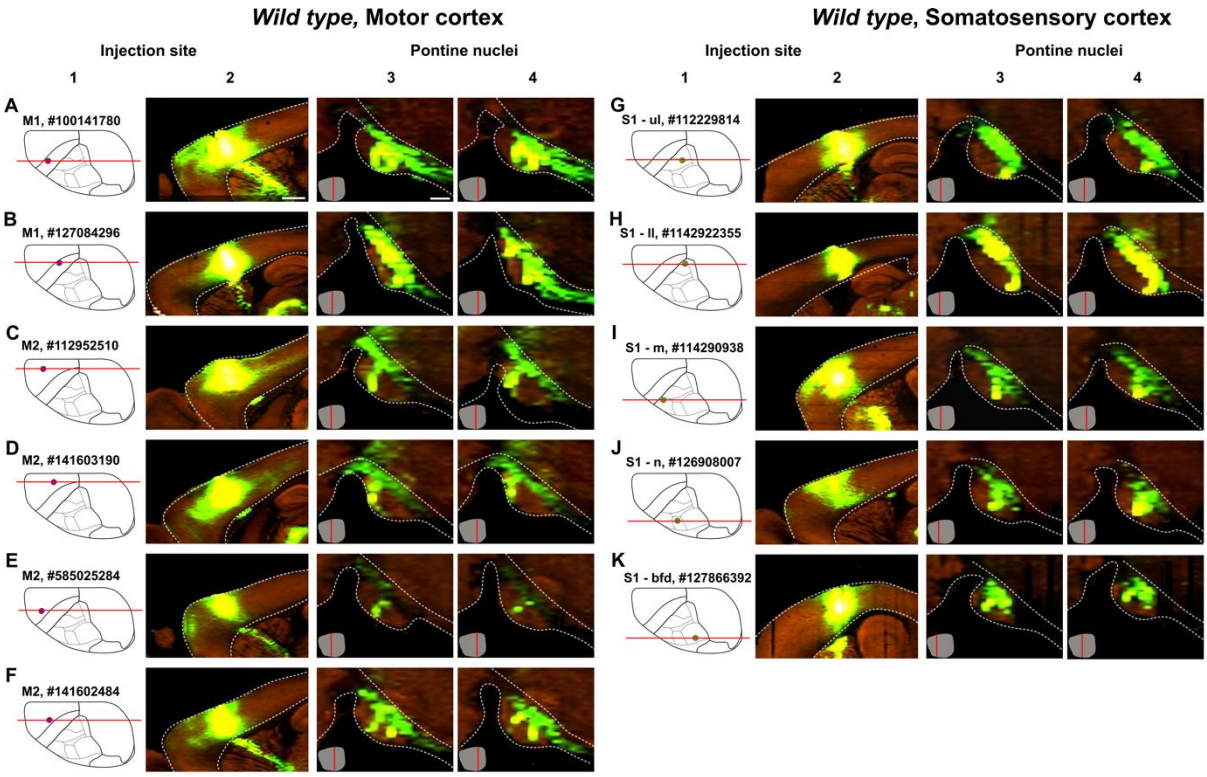

Fig. S3. Overview of tract-tracing experiments in wild-type mice

(**A-K**) Sagittally-oriented fluorescence microscopy images showing all wild-type C57BL/6J mouse tract-tracing data captured from the online image viewer of the Allen Mouse Brain Connectivity Atlas. **Column 1** shows dorsal view diagrams of the cerebral cortex indicating the position of the tracer injection site as a red dot, and a red line indicating the location of the sagittal images in **column 2** that show injection site centres. Letters and numbers indicate injected cortical area and ID numbers. **Columns 3 and 4** show fluorescence microscopy images of sagittal sections through the pontine nuclei, showing representative corticopontine labelling at two mediolateral levels as indicated with red lines on the inset ventral view diagram of the pontine nuclei. Abbreviations, bfd, barrel field; M1, primary motor cortex; M2, secondary motor cortex; ll, lower limb; m, mouth; n, nose; ul, upper limb. Scale bars, 1mm (column 2), 200µm (columns 3, 4).

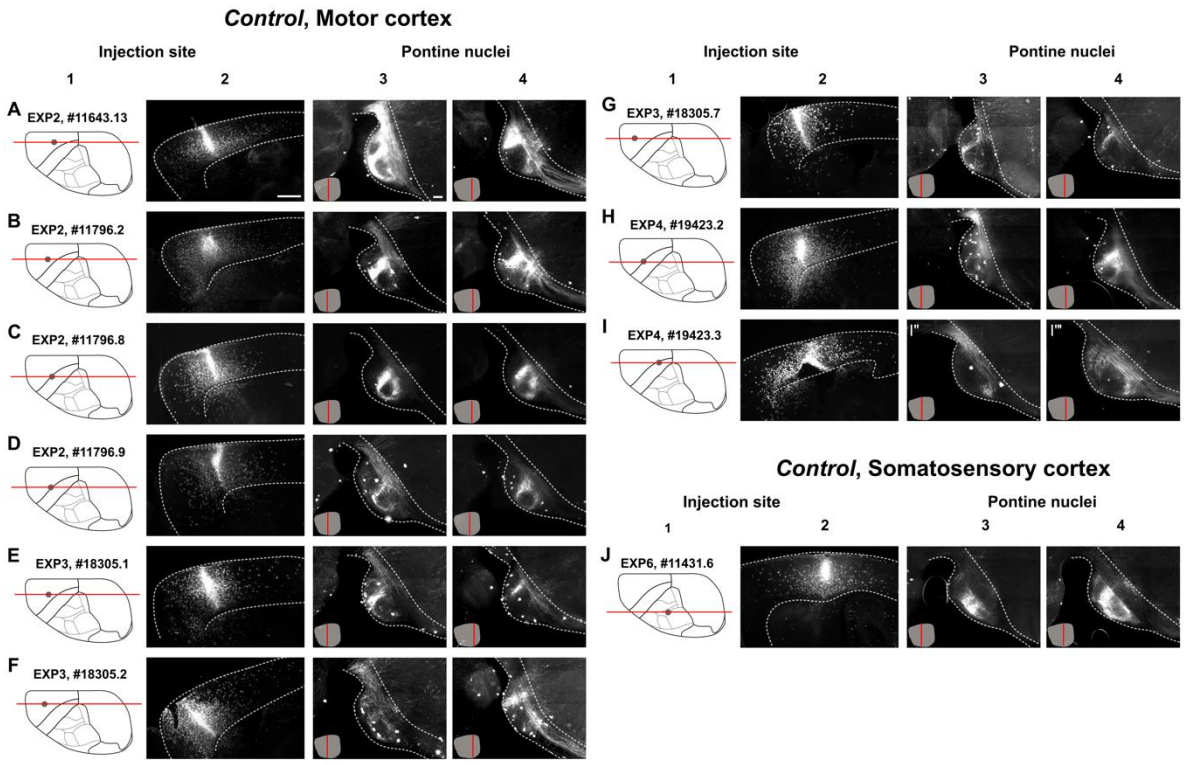

Fig. S4. Overview of tract-tracing experiments in control mice

(**A-J**) Sagittally-oriented fluorescence microscopy images showing all tract-tracing data conducted in control animals. **Column 1** shows dorsal view diagrams of the cerebral cortex indicating the position of the tracer injection site as a red dot, and a red line indicating the location of the sagittal images in **column 2** that show injection site centres. Letters and numbers indicate injected cortical area and ID numbers. **Columns 3 and 4** show fluorescence microscopy images of sagittal sections through the pontine nuclei, showing representative corticopontine labelling at two mediolateral levels as indicated with red lines on the inset ventral view diagram of the pontine nuclei. Scale bars, 1mm (column 2), 200µm (columns 3, 4).

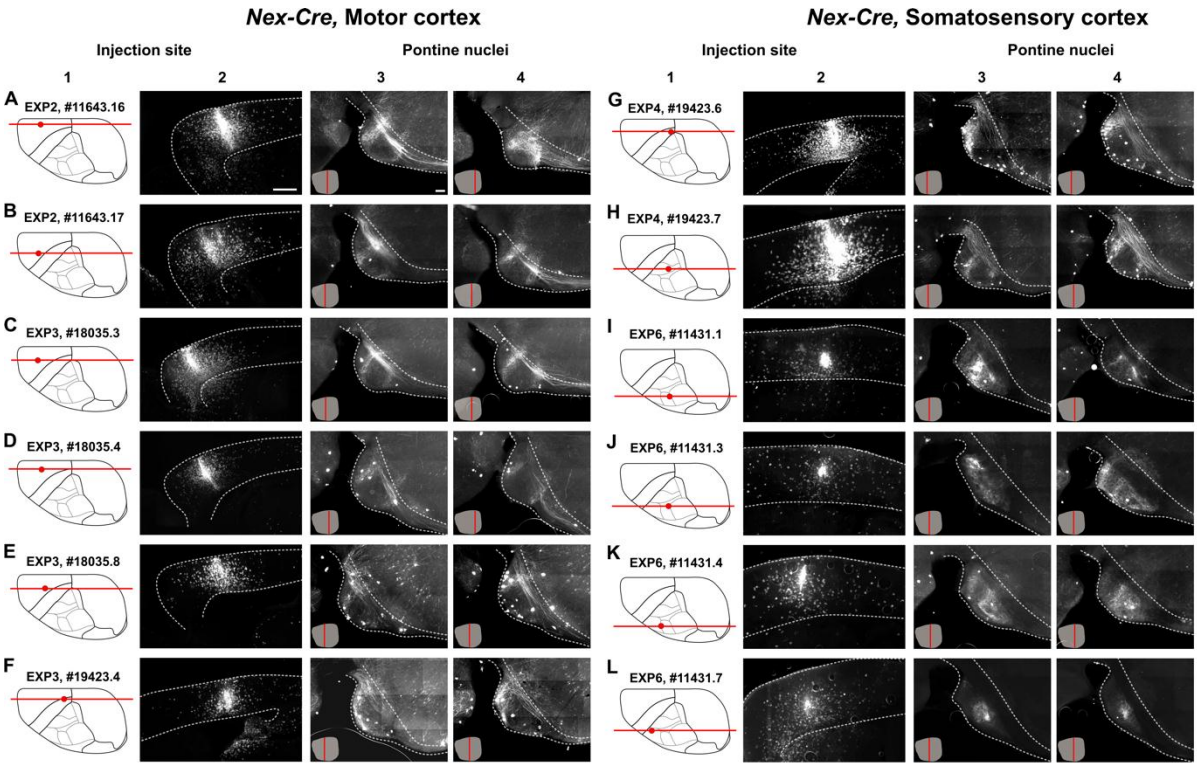

Fig. S5. Overview of tract-tracing experiments in *Nex-cKO* mice

(**A-L**) Sagittally-oriented fluorescence microscopy images showing all tract-tracing data conducted in *Nex-cKO* animals. **Column 1** shows dorsal view diagrams of the cerebral cortex indicating the position of the tracer injection site as a red dot, and a red line indicating the location of the sagittal images in **column 2** that show injection site centres. Letters and numbers indicate injected cortical area and ID numbers. **Columns 3 and 4** show fluorescence microscopy images of sagittal sections through the pontine nuclei, showing representative corticopontine labelling at two mediolateral levels as indicated with red lines on the inset ventral view diagram of the pontine nuclei. Scale bars, 1mm (column 2), 200µm (columns 3, 4).

Table S1. Overview of wild-type experiments from the Allen Mouse Brain Connectivity database

Allen Mouse Brain Connectivity database					
Experiment number #	**Sex**	**Age (±2)**	**Genotype**	**Injection site**	**Shown in**
100141780	Male	P56	C57BL/6J	Primary motor cortex	Fig. 2, 6A-F
114290938	male	P56	C57BL/6J	Primary somatosensory cortex, mouth region	Fig. 2A-P, 7A and 7H
112229814	male	P56	C57BL/6J	Primary somatosensory cortex, upper limb region	Fig. 2, 7B and 7F
112952510	male	P56	C57BL/6J	Secondary motor cortex	Fig. 2
114292355	male	P56	C57BL/6J	Primary somatosensory cortex, lower limb region	Fig. 2, 7A and 7D
126908007	male	P56	C57BL/6J	Primary somatosensory cortex, nose region	Fig. 2, 7A and 7G
127084296	male	P56	C57BL/6J	Secondary motor cortex	Fig. 2
127866392	male	P56	C57BL/6J	Primary somatosensory cortex, barrel field region	Fig. 2
141602484	male	P56	C57BL/6J	Secondary motor cortex	Fig. 2
141603190	male	P56	C57BL/6J	Secondary motor cortex	Fig. 2
585025284	male	P56	C57BL/6J	Secondary motor cortex	Fig. 2

Table S2. Overview of *Emx1-cKO* and *Nex-cKO* mice

Adult					
Exp. #	**Animal #**	**Sex**	**Age**	**Genotype**	**Shown in**
1	13588	female	P33	*Thy1-eYFP$^{T/+}$; Nr2f1$^{fl/fl}$*	Fig. 3, 4, 5 and Suppl. Fig.1, 2
1	13587	female	P33	*Thy1-eYFP$^{T/+}$; Nr2f1$^{fl/fl}$; Nex-Cre*	Fig. 3, 4, 5 and Suppl. Fig.1, 2
2	13585	male	P62	*Thy1-eYFP$^{T/+}$; Nr2f1$^{fl/fl}$; Nex-Cre*	Fig. 3, 4, 5 and Suppl. Fig.1, 2
3	13809	male	P57	*Thy1-eYFP$^{T/+}$; Nr2f1$^{fl/fl}$; Nex-Cre*	Fig. 3, 4, 5 and Suppl. Fig.1, 2
4	14258	male	P57	*Thy1-eYFP$^{T/+}$; Nr2f1$^{fl/fl}$*	Fig. 3, 4, 5 and Suppl. Fig.1, 2
4	14260	male	P57	*Thy1-eYFP$^{T/+}$; Nr2f1$^{fl/fl}$; Nex-Cre*	Fig. 3, 4, 5 and Suppl. Fig.1, 2
5	13805	male	P55	*Thy1-eYFP$^{T/+}$; Nr2f1$^{fl/fl}$; Nex-Cre*	Fig. 3, 4, 5 and Suppl. Fig.1, 2
5	14250	male	P72	*Thy1-eYFP$^{T/+}$; Nr2f1$^{fl/fl}$*	Fig. 3, 4, 5 and Suppl. Fig.1, 2
5	15170	male	P75	*Thy1-eYFP$^{T/+}$; Nr2f1$^{fl/fl}$*	Fig. 3, 4, 5 and Suppl. Fig.1, 2
6	16922	male	P76	*Thy1-eYFP$^{T/+}$; Nr2f1$^{fl/fl}$; Emx1-Cre*	Fig. 3, 4, 5 and Suppl. Fig.1, 2
6	16923	male	P76	*Thy1-eYFP$^{T/+}$; Nr2f1$^{fl/fl}$*	Fig. 3, 4, 5 and Suppl. Fig.1, 2
6	16924	male	P76	*Thy1-eYFP$^{T/+}$; Nr2f1$^{fl/fl}$*	Fig. 3, 4, 5 and Suppl. Fig.1, 2
6	16926	male	P76	*Thy1-eYFP$^{T/+}$; Nr2f1$^{fl/fl}$; Emx1-Cre*	Fig. 3, 4, 5 and Suppl. Fig.1, 2
7	17882	male	P72	*Thy1-eYFP$^{T/+}$; Nr2f1$^{fl/fl}$; Emx1-Cre*	Fig. 3, 4, 5 and Suppl. Fig.1, 2
8	18046	female	P109	*Thy1-eYFP$^{T/+}$; Nr2f1$^{fl/fl}$; Emx1-Cre*	Fig. 3, 4, 5 and Suppl. Fig.1, 2
8	18166	female	P98	*Thy1-eYFP$^{T/+}$; Nr2f1$^{fl/fl}$*	Fig. 3, 4, 5 and Suppl. Fig.1, 2
8	18271	female	P87	*Thy1-eYFP$^{T/+}$; Nr2f1$^{fl/fl}$*	Fig. 3, 4, 5 and Suppl. Fig.1, 2
9	19606	female	P86	*Thy1-eYFP$^{T/+}$; Nr2f1$^{fl/fl}$; Emx1-Cre*	Fig. 4
9	19607	female	P86	*Thy1-eYFP$^{T/+}$; Nr2f1$^{fl/fl}$; Emx1-Cre*	Fig. 4

Table S3. Overview of tract tracing experiments in *Nex-cKO* and *Ctrl* mice

P21 – unilateral CST tracing			
Tracer injected in motor cortex			
Experiment #	**Animal #**	**Genotype**	**Shown in**
2	11643_13	*Ctrl*	Fig. 6A and 7B
2	11643_16	*Nex-cKO*	Suppl. Fig. 3
2	11643_17	*Nex-cKO*	Fig. 6A and 6F
2	11796_2	*Ctrl*	Suppl. Fig. 3
2	11796_8	*Ctrl*	Suppl. Fig. 3
2	11796_9	*Ctrl*	Suppl. Fig. 3
3	18035_1	*Ctrl*	Fig. 6A and 6F
3	18035_2	*Ctrl*	Fig. 6A and 6E
3	18035_7	*Ctrl*	Suppl. Fig. 3
3	18035_3	*Nex-cKO*	Fig. 6A and 6E
3	18035_4	*Nex-cKO*	Suppl. Fig. 3
3	18035_8	*Nex-cKO*	Fig. 6A and 76D
4	19423_2	*Ctrl*	Suppl. Fig. 3
4	19423_3	*Ctrl*	Suppl. Fig. 3
4	19423_4	*Nex-cKO*	Suppl. Fig. 3
4	19423_5	*Nex-cKO*	Suppl. Fig. 3
Tracer injected in somatosensory cortex			
4	19423_6	*Nex-cKO*	Fig. 7A and 7D
4	19423_7	*Nex-cKO*	Fig. 7A and 7E
6	11431_1	*Nex-cKO*	Fig. 7A and 7G
6	11431_3	*Nex-cKO*	Fig. 7A and 7H
6	11431_4	*Nex-cKO*	Fig. 7A and 7F
6	11431_6	*Ctrl*	Fig. 7A and 7F
6	11431_7	*Nex-cKO*	Fig. 7A and 7H

Table S4. Overview of quantitative results.

Highlighted in blue, comparisons that produced statistically significant P-values. P-values are calculated by 2way ANOVA test (**Figures 3F,G and 4E-F**), or ordinary one-way ANOVA test (**Figures 4G-I**).

Figure 3B"-D"– Cortical distribution of YFP-H positive cells (% values)							
Area	**Hypothesis**	**Mean 1**	**Mean 2**	**Mean diff.**	**95,00% CI of diff**	**Summary**	**Adjusted P.**
PFC	*Ctrl vs. Nex-cKO*	4.833	1.95	2.883	-3.655 to 9.421	ns	0.5437
	Ctrl vs. Emx1-cKO	4.833	3.15	1.683	-4.855 to 8.221	ns	0.8112
	Nex-cKO vs. Emx1-cKO	1.95	3.15	-1.2	-8.362 to 5.962	ns	0.9150
M	*Ctrl vs. Nex-cKO*	46.87	24.69	22.18	15.64 to 28.71	****	<0.0001
	Ctrl vs. Emx1-cKO	46.87	27.08	19.78	13.25 to 26.32	****	<0.0001
	Nex-cKO vs. Emx1-cKO	24.69	27.08	-2.393	-9.555 to 4.769	ns	0.7036
S	*Ctrl vs. Nex-cKO*	23.25	27.56	-4.312	-10.85 to 2.226	ns	0.2608
	Ctrl vs. Emx1-cKO	23.25	23.42	-0.1744	-6.712 to 6.363	ns	0.9977
	Nex-cKO vs. Emx1-cKO	27.56	23.42	4.137	-3.024 to 11.3	ns	0.3545
A	*Ctrl vs. Nex-cKO*	5.671	8.786	-3.115	-9.653 to 3.423	ns	0.4917
	Ctrl vs. Emx1-cKO	5.671	5.947	-0.2756	-6.813 to 6.262	ns	0.9944
	Nex-cKO vs. Emx1-cKO	8.786	5.947	2.839	-4.323 to 10	ns	0.6105
V	*Ctrl vs. Nex-cKO*	10.13	21.5	-11.36	-17.9 to -4.825	***	0.0003
	Ctrl vs. Emx1-cKO	10.13	21.35	-11.22	-17.76 to -4.681	***	0.0003
	Nex-cKO vs. Emx1-cKO	21.5	21.35	0.1434	-7.018 to 7.305	ns	0.9987
RSC	*Ctrl vs. Nex-cKO*	9.184	15.5	-6.318	-12.86 to 0.2199	ns	0.0604
	Ctrl vs. Emx1-cKO	9.184	19.01	-9.821	-16.36 to -3.284	**	0.0017
	Nex-cKO vs. Emx1-cKO	15.5	19.01	-3.503	-10.67 to 3.658	ns	0.4734
Figure 3E– Cortical distribution of YFP-H positive cells (#of cells/slides)							
Area	**Hypothesis**	**Mean 1**	**Mean 2**	**Mean diff.**	**95,00% CI of diff**	**Summary**	**Adjusted P.**
PFC	*Ctrl vs. Nex-cKO*	*33.06*	*6.42*	*26.64*	*-52.67 to 105.9*	*ns*	*0.5048*
	Ctrl vs. Emx1-cKO	*33.06*	*40.33*	*-7.269*	*-86.57 to 72.03*	*ns*	*0.8553*
	Nex-cKO vs. Emx1-cKO	*6.42*	*40.33*	*-33.91*	*-120.8 to 52.96*	*ns*	*0.4386*
M	*Ctrl vs. Nex-cKO*	*324.5*	*91.87*	*232.6*	*153.3 to 311.9*	****	*<0.0001*
	Ctrl vs. Emx1-cKO	*324.5*	*301.7*	*22.78*	*-56.52 to 102.1*	*ns*	*0.5682*
	Nex-cKO vs. Emx1-cKO	*91.87*	*301.7*	*-209.9*	*-296.7 to -123*	****	*<0.0001*
S	*Ctrl vs. Nex-cKO*	*163.2*	*105.2*	*57.98*	*-21.32 to 137.3*	*ns*	*0.1491*
	Ctrl vs. Emx1-cKO	*163.2*	*257.8*	*-94.58*	*-173.9 to -15.28*	*	*0.0202*
	Nex-cKO vs. Emx1-cKO	*105.2*	*257.8*	*-152.6*	*-239.4 to -65.69*	***	*0.0008*
A	*Ctrl vs. Nex-cKO*	*38.09*	*32.77*	*5.32*	*-73.98 to 84.62*	*ns*	*0.8939*
	Ctrl vs. Emx1-cKO	*38.09*	*61.63*	*-23.53*	*-102.8 to 55.77*	*ns*	*0.5555*
	Nex-cKO vs. Emx1-cKO	*32.77*	*61.63*	*-28.85*	*-115.7 to 58.02*	*ns*	*0.5095*

V	*Ctrl vs. Nex-cKO*	*81.24*	*81.07*	*0.1681*	*-79.13 to 79.47*	*ns*	*0.9966*
	Ctrl vs. Emx1-cKO	*81.24*	*228*	*-146.8*	*-226.1 to -67.45*	***	*0.0004*
	Nex-cKO vs. Emx1-cKO	*81.07*	*228*	*-146.9*	*-233.8 to -60.05*	**	*0.0012*
RSC	*Ctrl vs. Nex-cKO*	*64.39*	*58.41*	*5.974*	*-73.33 to 85.28*	*ns*	*0.8809*
	Ctrl vs. Emx1-cKO	*64.39*	*204.1*	*-139.8*	*-219.1 to -60.46*	***	*0.0008*
	Nex-cKO vs. Emx1-cKO	*58.41*	*204.1*	*-145.7*	*-232.6 to -58.86*	**	*0.0013*

Figure 3F– Distribution of YFP-H positive cells among M and S areas (% values)

Area	Hypothesis	Mean 1	Mean 2	Mean diff.	95,00% CI of diff	Summary	Adjusted P.
M	*Ctrl vs. Nex-cKO*	*66.85*	*47.35*	*19.5*	*7.864 to 31.14*	**	*0.0021*
	Ctrl vs. Emx1-cKO	*66.85*	*53.43*	*13.43*	*1.79 to 25.07*	*	*0.0257*
	Nex-cKO vs. Emx1-cKO	*47.35*	*53.43*	*-6.074*	*-18.82 to 6.676*	*ns*	*0.3339*
S	*Ctrl vs. Nex-cKO*	*33.15*	*52.65*	*-19.5*	*-31.14 to -7.864*	**	*0.0021*
	Ctrl vs. Emx1-cKO	*33.15*	*46.57*	*-13.43*	*-25.07 to -1.79*	*	*0.0257*
	Nex-cKO vs. Emx1-cKO	*52.65*	*46.57*	*6.074*	*-6.676 to 18.82*	*ns*	*0.3339*

Figure 4E – Rostral LFP diameter

Section	Hypothesis	Mean 1	Mean 2	Mean diff.	95,00% CI of diff	Summary	Adjusted P.
1	*Ctrl vs. Nex-cKO*	0	0	0	-116.9 to 116.9	ns	>0.9999
	Ctrl vs. Emx1-cKO	0	0	0	-116.9 to 116.9	ns	>0.9999
	Nex-cKO vs. Emx1-cKO	0	0	0	-124.9 to 124.9	ns	>0.9999
2	*Ctrl vs. Nex-cKO*	0	28.29	-28.29	-145.2 to 88.57	ns	0.836
	Ctrl vs. Emx1-cKO	0	0	0	-116.9 to 116.9	ns	>0.9999
	Nex-cKO vs. Emx1-cKO	28.29	0	28.29	-96.64 to 153.2	ns	0.8549
3	*Ctrl vs. Nex-cKO*	0	132.7	-132.7	-249.6 to -15.84	*	0.0215
	Ctrl vs. Emx1-cKO	0	0	0	-116.9 to 116.9	ns	>0.9999
	Nex-cKO vs. Emx1-cKO	132.7	0	132.7	7.775 to 257.6	*	0.0343
4	*Ctrl vs. Nex-cKO*	0	179.6	-179.6	-296.5 to -62.77	**	0.001
	Ctrl vs. Emx1-cKO	0	0	0	-116.9 to 116.9	ns	>0.9999
	Nex-cKO vs. Emx1-cKO	179.6	0	179.6	54.71 to 304.6	**	0.0023
5	*Ctrl vs. Nex-cKO*	0	175.9	-175.9	-292.8 to -59.04	**	0.0013
	Ctrl vs. Emx1-cKO	0	55.34	-55.34	-172.2 to 61.52	ns	0.5052
	Nex-cKO vs. Emx1-cKO	175.9	55.34	120.6	-4.369 to 245.5	ns	0.0612
6	*Ctrl vs. Nex-cKO*	24.35	169.6	-145.2	-262.1 to -28.37	*	0.0103
	Ctrl vs. Emx1-cKO	24.35	115	-90.67	-207.5 to 26.2	ns	0.1624
	Nex-cKO vs. Emx1-cKO	169.6	115	54.57	-70.37 to 179.5	ns	0.5592
7	*Ctrl vs. Nex-cKO*	117	231.4	-114.4	-231.3 to 2.467	ns	0.0565
	Ctrl vs. Emx1-cKO	117	234.6	-117.7	-234.5 to 0.8201	*	0.048
	Nex-cKO vs. Emx1-	231.4	234.6	-3.287	-128.2 to 121.6	ns	0.9979

	cKO						
8	*Ctrl vs. Nex-cKO*	241.7	187.5	54.13	-66.26 to 174.5	ns	0.5401
	Ctrl vs. Emx1-cKO	241.7	293	-51.33	-171.7 to 69.06	ns	0.5746
	Nex-cKO vs. Emx1-cKO	187.5	293	-105.5	-230.4 to 19.47	ns	0.1168
9	*Ctrl vs. Nex-cKO*	316.6	267.9	48.71	-68.15 to 165.6	ns	0.5888
	Ctrl vs. Emx1-cKO	316.6	250.1	66.55	-56.81 to 189.9	ns	0.4128
	Nex-cKO vs. Emx1-cKO	267.9	250.1	17.83	-113.2 to 148.9	ns	0.9449
10	*Ctrl vs. Nex-cKO*	318.9	194.4	124.6	7.715 to 241.4	*	0.0335
	Ctrl vs. Emx1-cKO	318.9	205.8	113.1	-3.738 to 230	ns	0.0602
	Nex-cKO vs. Emx1-cKO	194.4	205.8	-11.45	-136.4 to 113.5	ns	0.9746
11	*Ctrl vs. Nex-cKO*	231.1	88.06	143.1	-163 to 449.1	ns	0.514
	Ctrl vs. Emx1-cKO	231.1	64.04	167.1	-82.79 to 416.9	ns	0.258
	Nex-cKO vs. Emx1-cKO	88.06	64.04	24.02	-225.8 to 273.9	ns	0.9721
12	*Ctrl vs. Nex-cKO*	276.1	179.6	96.5	-26.86 to 219.9	ns	0.1576
	Ctrl vs. Emx1-cKO	276.1	136.5	139.6	16.23 to 263	*	0.022
	Nex-cKO vs. Emx1-cKO	179.6	136.5	43.09	-93.77 to 179.9	ns	0.7389
13	*Ctrl vs. Nex-cKO*	201.9	180.5	21.33	-243.7 to 286.3	ns	0.9804
	Ctrl vs. Emx1-cKO	201.9	44.45	157.4	-40.14 to 354.9	ns	0.1471
	Nex-cKO vs. Emx1-cKO	180.5	44.45	136.1	-113.8 to 385.9	ns	0.4059
14	*Ctrl vs. Nex-cKO*	218.4	114.6	103.8	-19.52 to 227.2	ns	0.1182
	Ctrl vs. Emx1-cKO	218.4	95.41	123	-0.3344 to 246.4	ns	0.0508
	Nex-cKO vs. Emx1-cKO	114.6	95.41	19.19	-117.7 to 156	ns	0.9416
15	*Ctrl vs. Nex-cKO*	154.7	59.11	95.61	-21.25 to 212.5	ns	0.1328
	Ctrl vs. Emx1-cKO	154.7	51.17	103.6	-13.31 to 220.4	ns	0.0942
	Nex-cKO vs. Emx1-cKO	59.11	51.17	7.94	-117 to 132.9	ns	0.9877
16	*Ctrl vs. Nex-cKO*	101.6	16.85	84.78	-32.09 to 201.6	ns	0.2035
	Ctrl vs. Emx1-cKO	101.6	18.75	82.87	-33.99 to 199.7	ns	0.2183
	Nex-cKO vs. Emx1-cKO	16.85	18.75	-1.908	-126.8 to 123	ns	0.9993
17	*Ctrl vs. Nex-cKO*	60.94	0	60.94	-55.93 to 177.8	ns	0.4374
	Ctrl vs. Emx1-cKO	60.94	0	60.94	-55.93 to 177.8	ns	0.4374
	Nex-cKO vs. Emx1-cKO	0	0	0	-124.9 to 124.9	ns	>0.9999
18	*Ctrl vs. Nex-cKO*	28.85	0	28.85	-88.02 to 145.7	ns	0.8301
	Ctrl vs. Emx1-cKO	28.85	0	28.85	-88.02 to 145.7	ns	0.8301
	Nex-cKO vs. Emx1-cKO	0	0	0	-124.9 to 124.9	ns	>0.9999
19	*Ctrl vs. Nex-cKO*	0	0	0	-112 to 112	ns	>0.9999
	Ctrl vs. Emx1-cKO	0	0	0	-116.9 to 116.9	ns	>0.9999
	Nex-cKO vs. Emx1-cKO	0	0	0	-120.4 to 120.4	ns	>0.9999

Figure 4F – Caudal LFP diameter

Section	Hypothesis	Mean 1	Mean 2	Mean diff.	95,00% CI of diff	Summary	Adjusted P.
1	*Ctrl vs. Nex-cKO*	0	0	0	-88.51 to 88.51	ns	>0.9999
	Ctrl vs. Emx1-cKO	0	0	0	-88.51 to 88.51	ns	>0.9999
	Nex-cKO vs. Emx1-	0	0	0	-94.62 to 94.62	ns	>0.9999

	cKO						
2	*Ctrl vs. Nex-cKO*	0	46.89	-46.89	-135.4 to 41.62	ns	0.4252
	Ctrl vs. Emx1-cKO	0	0	0	-88.51 to 88.51	ns	>0.9999
	Nex-cKO vs. Emx1-cKO	46.89	0	46.89	-47.73 to 141.5	ns	0.4728
3	*Ctrl vs. Nex-cKO*	0	98.1	-98.1	-186.6 to -9.584	*	0.0257
	Ctrl vs. Emx1-cKO	0	0	0	-88.51 to 88.51	ns	>0.9999
	Nex-cKO vs. Emx1-cKO	98.1	0	98.1	3.473 to 192.7	*	0.0402
4	*Ctrl vs. Nex-cKO*	0	126.2	-126.2	-214.7 to -37.72	**	0.0026
	Ctrl vs. Emx1-cKO	0	0	0	-88.51 to 88.51	ns	>0.9999
	Nex-cKO vs. Emx1-cKO	126.2	0	126.2	31.6 to 220.9	**	0.0053
5	*Ctrl vs. Nex-cKO*	18.5	111	-92.51	-181 to -3.999	*	0.0382
	Ctrl vs. Emx1-cKO	18.5	13.31	5.196	-83.32 to 93.71	ns	0.9895
	Nex-cKO vs. Emx1-cKO	111	13.31	97.71	3.084 to 192.3	*	0.0412
6	*Ctrl vs. Nex-cKO*	69.28	128.1	-58.82	-147.3 to 29.69	ns	0.2617
	Ctrl vs. Emx1-cKO	69.28	97.47	-28.19	-116.7 to 60.32	ns	0.7331
	Nex-cKO vs. Emx1-cKO	128.1	97.47	30.63	-63.99 to 125.3	ns	0.7256
7	*Ctrl vs. Nex-cKO*	107.5	176	-68.56	-300.3 to 163.2	ns	0.765
	Ctrl vs. Emx1-cKO	107.5	152.1	-44.66	-227.9 to 138.6	ns	0.8336
	Nex-cKO vs. Emx1-cKO	176	152.1	23.9	-159.3 to 207.1	ns	0.9491
8	*Ctrl vs. Nex-cKO*	175.2	237.2	-61.95	-157.9 to 34.02	ns	0.2821
	Ctrl vs. Emx1-cKO	175.2	154.5	20.69	-70.49 to 111.9	ns	0.8541
	Nex-cKO vs. Emx1-cKO	237.2	154.5	82.63	-16.61 to 181.9	ns	0.1235
9	*Ctrl vs. Nex-cKO*	214.5	138.2	76.34	-12.17 to 164.9	ns	0.1063
	Ctrl vs. Emx1-cKO	214.5	197.7	16.82	-71.69 to 105.3	ns	0.8952
	Nex-cKO vs. Emx1-cKO	138.2	197.7	-59.52	-154.1 to 35.1	ns	0.3005
10	*Ctrl vs. Nex-cKO*	209.6	115.1	94.49	5.983 to 183	*	0.0333
	Ctrl vs. Emx1-cKO	209.6	132	77.6	-10.91 to 166.1	ns	0.0988
	Nex-cKO vs. Emx1-cKO	115.1	132	-16.89	-111.5 to 77.73	ns	0.9069
11	*Ctrl vs. Nex-cKO*	232.5	99.13	133.4	44.9 to 221.9	**	0.0013
	Ctrl vs. Emx1-cKO	232.5	116.2	116.4	27.87 to 204.9	**	0.0061
	Nex-cKO vs. Emx1-cKO	99.13	116.2	-17.03	-111.7 to 77.59	ns	0.9055
12	*Ctrl vs. Nex-cKO*	186.4	127.8	58.65	-34.78 to 152.1	ns	0.302
	Ctrl vs. Emx1-cKO	186.4	26.38	160.1	71.56 to 248.6	****	<0.0001
	Nex-cKO vs. Emx1-cKO	127.8	26.38	101.4	2.179 to 200.7	*	0.0439
13	*Ctrl vs. Nex-cKO*	94.47	0	94.47	-137.3 to 326.2	ns	0.6019
	Ctrl vs. Emx1-cKO	94.47	13.38	81.09	-95.93 to 258.1	ns	0.527
	Nex-cKO vs. Emx1-cKO	0	13.38	-13.38	-190.4 to 163.6	ns	0.9826
14	*Ctrl vs. Nex-cKO*	58.1	0	58.1	-33.08 to 149.3	ns	0.2913
	Ctrl vs. Emx1-cKO	58.1	0	58.1	-33.08 to 149.3	ns	0.2913
	Nex-cKO vs. Emx1-cKO	0	0	0	-94.62 to 94.62	ns	>0.9999
15	*Ctrl vs. Nex-cKO*	0	0	0	-84.82 to 84.82	ns	>0.9999

	Ctrl vs. Emx1-cKO	0	0	0	-88.51 to 88.51	ns	>0.9999
	Nex-cKO vs. Emx1-cKO	0	0	0	-91.18 to 91.18	ns	>0.9999
Figure 4G – Rostral LFP area							
	Hypothesis	**Mean 1**	**Mean 2**	**Mean diff.**	**95,00% CI of diff**	**Summary**	**Adjusted P.**
	Ctrl vs. Nex-cKO	2414	2258	156.4	-570.3 to 883	ns	0.8257
	Ctrl vs. Emx1-cKO	2414	1725	689.2	-37.42 to 1416	ns	0.0637
Figure 4H – Caudal LFP area							
	Hypothesis	**Mean 1**	**Mean 2**	**Mean diff.**	**95,00% CI of diff**	**Summary**	**Adjusted P.**
	Ctrl vs. Nex-cKO	1403	1427	-24.29	-261.8 to 213.2	ns	0.9566
	Ctrl vs. Emx1-cKO	1403	884.1	518.8	281.3 to 756.3	***	0.0001
Figure 4I – Fasciculation Index							
Region	**Hypothesis**	**Mean 1**	**Mean 2**	**Mean diff.**	**95,00% CI of diff**	**Summary**	**Adjusted P.**
250 μm	*Ctrl vs. Nex-cKO*	0.6528	0.5493	0.1035	0.01185 to 0.1951	*	0.0216
	Ctrl vs. Emx1-cKO	0.6528	0.5595	0.09326	0.001658 to 0.1849	*	0.0446
500 μm	*Ctrl vs. Nex-cKO*	0.674	0.5771	0.0969	0.00254 to 0.1913	*	0.0422
	Ctrl vs. Emx1-cKO	0.674	0.5146	0.1594	0.06502 to 0.2537	***	0.0004

Table S5. List of primary and secondary antibodies used in this study.

Antigen	Provider	Catalog #	Species	Working dilution
GFP	Abcam	Ab13970	Ck	1:500
RFP	Abcam	Ab 124754	Rb	1:500
Ck IgY - AF 488	Thermo Fisher	A11039	Gt	1:500
Rb IgG - AF 555	Thermo Fisher	A21428	Gt	1:500

Table S6. Raw data and statistical analyses related to Table S4.

Click here to download Table S6